Engineered geopolymer composites: A state-of-the-art review

Hui Zhong, Mingzhong Zhang*

Department of Civil, Environmental and Geomatic Engineering, University College London, London, WC1E 6BT, UK

Abstract: Engineered cementitious composite (ECC) featuring extraordinary tensile ductility is a promising option for many structural applications but its large-scale manufacture is not eco-friendly due to its binding ingredient, Portland cement. One of the potential alternatives to ECC is engineered geopolymer composites (EGC) that have been increasingly studied in recent years. This paper presents a comprehensive review of the state-of-the-art of EGC in terms of design theory, mix design, fabrication process, engineering properties, durability and environmental benefit, with special focus on the effects of different material composition factors including precursor, activator, aggregate, additive and fibre on the critical material properties of EGC especially uniaxial tensile properties. The correlations between essential mechanical properties are discussed in depth. The unique tensile behaviour of EGC can be tailored by modifying the material composition that would change its internal microstructure and in turn alter the matrix properties and fibre-matrix interfacial behaviour. Compared to typical ECC, around 64% of EGC mixtures have higher tensile strain capacity (over 2.49%) and about 27% of mixtures exhibit larger tensile strength (over 4.86 MPa). Through adjusting the mix design of EGC, it holds promises as a cost-effective and sustainable material for applications against dynamic loadings, fire and chemical attacks, as well as 3D concrete printing. This review summarises the recent advances in EGC and identifies the remaining challenges in development of EGC with desired properties for practical applications.

Keywords: Strain-hardening geopolymer composites; Fibre reinforced concrete; Micromechanics; Mechanical properties; Durability; Sustainability

1. Introduction

Concrete is the most widely used construction material in the world, which is strong in compression but weak in tension with tensile strain capacity of only about 0.01% [1]. To suppress this weakness, an increasing number of studies have focused on the development of fibre reinforced cementitious composites since 1960s [2]. However, as seen in Fig. 1, ordinary fibre reinforced concrete (FRC) can lead to higher tensile strength than normal concrete but insufficient enhancement in tensile strain capacity. To achieve superior tensile ductility, engineered cementitious composites (ECC) were developed in the early 1990s, featuring strain-hardening and multiple cracking behaviour [1]. Unlike normal concrete and normal FRC, ECC strain-hardens after the formation of the first crack and has tensile strain capacity of several hundred times higher than normal concrete and FRC. ECC exhibits

* Corresponding author. E-mail address: mingzhong.zhang@ucl.ac.uk (M. Zhang)

self-controlled crack widths under loading state, where the initial cracks stop widening after exceeding about 1% tensile strain and the further tensile deformation is induced by the generation of new micro-cracks [3]. Because of these unique characteristics, ECC has been applied in various full-scale structures such as bridges and high-rise buildings to prolong the service life and offer improved functions [4-6].

The typical ECC is made from Portland cement, supplementary cementitious materials (e.g., fly ash (FA)), silica sand and short fibres, which contains about 2-3 times higher cement content than ordinary concrete due to the absence of coarse aggregates [7]. The production of Portland cement accounts for around 8% of the global CO_2 emissions [8], implying that the increasing development of ECC would hinder the sustainable development of construction industry. Therefore, it is vital to find alternative green binders for ECC. In recent years, geopolymers (also called alkali-activated materials) made from aluminosilicate source materials and alkaline activators were utilised as binders to develop engineered geopolymer composites (EGC) that are considered as a promising substitute for ECC. Compared to normal Portland cement concrete, geopolymer concrete can achieve comparable or even more superior mechanical properties and durability but around 50-80% less CO_2 emissions [9, 10]. In comparison with ECC, the developed EGC is more sustainable and has similar tensile and flexural properties under static loading but better mechanical properties under dynamic loading [11-14]. Like ECC, EGC in existing literature was developed based on the micromechanical design theory and can be prepared with different matrices, fibre reinforcements, and mixing and curing methods, leading to considerably different material properties. Therefore, it is vital to comprehensively review the current knowledge adopted in the material design of EGC. Although some material properties of EGC and potential research opportunities were discussed in Ref. [15], as a complement to the existing review, this review is mainly focused on the effects of different material composition factors and preparation methods on the engineering properties and durability of EGC especially uniaxial tensile behaviour, as well as the correlations between important mechanical properties, which have not been comprehensively reviewed. Based on this, the remaining challenges in developing EGC with desired properties for engineering applications can be identified.

This paper aims to present a critical review on the recent advances in the development of EGC, mainly focusing on the mix design, fabrication process, engineering properties, durability, and environmental benefits. The raw materials, mix design, mixing process, and curing regime of EGC are firstly introduced, followed by an overview of its design theory including two indices that govern the tensile strain-hardening behaviour, and the discussion on the key micromechanical model parameters affecting the tensile behaviour of EGC, as well as their relations to the strain-hardening indices. Then, the effects of different factors associated with matrix, fibre and curing on the fresh properties, drying shrinkage, mechanical properties, bond and self-healing performance, and

durability of EGC are critically reviewed, with special focus on the uniaxial tensile behaviour and the relationships between critical mechanical properties. Afterwards, the potential of utilising EGC in 3D concrete printing is discussed, followed by a comparison of sustainability between ECC and EGC in terms of carbon emission, energy consumption and material cost.

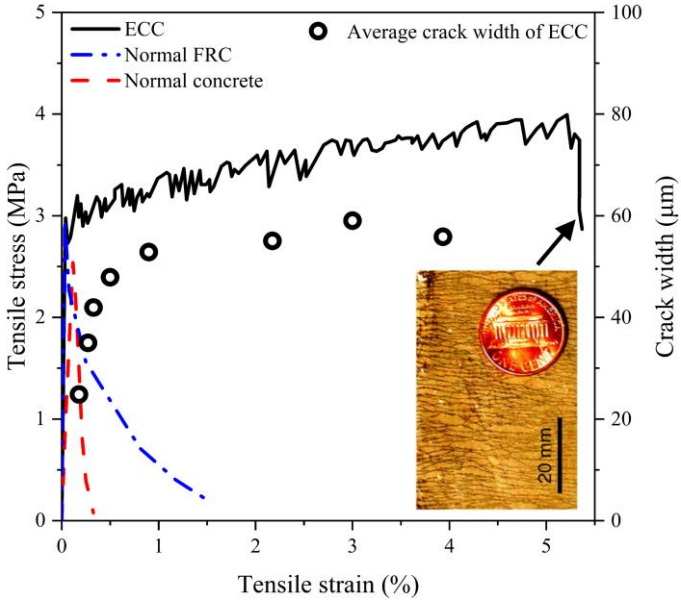

Fig. 1. Typical stress-strain curves of ECC, FRC and normal concrete [3, 16].

2. Composition and production

2.1. Raw materials and mix design

As mentioned above, geopolymers are produced via the reaction between aluminosilicate raw materials (i.e., precursors) and alkaline activators, where their reaction process can be divided as [17]: (1) dissolution, (2) rearrangement, (3) gel nucleation, and (4) solidification. When the raw binder materials are in contact with the alkaline activator, the surface bonds of the binders (e.g., Si-O-Si and Al-O-Al bonds in FA, CaO and Si-O-Si bonds in slag) are ruptured to generate a variety of dissolved species (e.g., silica, alumina and calcium monomers) [18, 19]. As the dissolution continues, these monomers would react with each other to form dimers, leading to the formation of 3D aluminosilicate gels. When a low-calcium precursor (e.g., FA) is used, the alkali aluminosilicate (N-A-S-H) gel is the main reaction product with a highly crosslinked disordered pseudo-zeolitic structure [20, 21], while the mixture containing a high-calcium precursor (e.g., slag) would primarily consist of calcium aluminosilicate hydrate (C-A-S-H) gel with a tobermorite-like structure [20, 22]. These gels can coexist if the precursors are blends of low-calcium and high-calcium binders [23].

Table 1 summarises the used raw materials, mixture design and curing regime for fabricating EGC. So far, different types of EGC have been developed using various precursors, activators, aggregates and fibres. FA, ground granulated blast-furnace slag (GGBS) and their blends were the frequently used precursors owing to their large availability and relatively stable chemical compositions [24, 25]. The commonly adopted contents of FA and GGBS were 50-80% and 20-50% (by the total mass of

binders) for the blended FA and GGSB system. About 6-19% silica fume (SF) can be incorporated into GGBS or blended FA and GGBS system to enhance the strength of EGC as a result of its fine particle size and pozzolanic reaction [26]. Metakaolin (MK) was used alone or along with FA (1.5%) to improve the overall properties of EGC because of its high active silica and alumina contents. Apart from the precursors above, ladle slag (LS) and steel slag (SS) from the steel-making process [27, 28], palm oil fuel ash (POFA) from the palm oil industry [29, 30], red mud (RM) generated during alumina extraction [31], incineration fly ash (IFA) from municipal solid waste incineration [32], rice husk ash (RHA) created via burning rice husk [33, 34], and liquid crystal display glass (LCDG) from the waste electronics [35] were also utilised to produce EGC for offering environmental benefits.

A combination of NaOH and Na_2SiO_3 was the most used liquid alkaline activator for EGC because of the relatively good excitation effect [36, 37]. The molarity of the used NaOH solution ranged from 4 M to 20 M, while the silicate modulus (SiO_2/Na_2O) of Na_2SiO_3 was in the range of 2.0-3.3. It should be mentioned that blending NaOH and Na_2SiO_3 solutions can release a large amount of heat, which requires a certain time to cool down before usage and is thereby time-consuming. Besides, it is not viable to handle a large quantity of corrosive alkaline solutions for large-scale applications. Hence, solid activators (e.g., anhydrous Na_2SiO_3) can be used instead, along with water during the mixing process, which can address some drawbacks of employing traditional liquid activators [38]. Most researchers have adopted liquid-to-binder ratios (L/b) ranging from 0.40 to 0.55 or water-to-solid ratios (W/s) of 0.20-0.35 for the mix design of EGC.

Similar to ECC, silica sand with average particle size of 100-236 μm and maximum particle size of less than 1180 μm was generally used as fine aggregate for EGC and coarse aggregate is inhibited as it can result in increased fracture toughness for the matrix (K_m) and therefore impair the unique tensile characteristics (i.e., strain-hardening and multiple cracking) of EGC [39]. To reduce the environmental impact induced by the overexploitation of natural resources and landfill of solid wastes such as waste tyres [40, 41], other types of aggregates including expanded glass, ceramic microsphere, expanded perlite, crumb rubber, and copper slag were employed to fully or partially replace the commonly used silica sand [34, 42, 43]. The aggregate-to-binder ratio (Agg/b) was normally controlled for obtaining a suitable K_m for the matrix and typically ranged from 0.2 to 0.5.

Different types of additives such as superplasticiser and viscosity modifying admixture were adopted to control the rheology of EGC's matrix as it can strongly affect the fibre distribution and orientation [44]. Additionally, defoamers or anti-foaming agents were used to reduce the formation of foam inside the EGC, which can change the internal pore structure, K_m and interfacial properties between matrix and fibre [45]. The contents of these additives were small, typically less than 1% of the total mass of the binder.

Like ECC, EGC contains randomly distributed short fibres at a dosage level of mostly no higher than 2.0%. Polyvinyl alcohol (PVA) fibre is a kind of synthetic fibre that has been widely used as fibre reinforcement in EGC due to its excellent mechanical properties, chemical resistance and easy dispersion [46]. Besides, as seen in Table 1, the diameter of the used PVA fibre is around 40 μm, which is small enough to improve the interfacial area between fibre and matrix for the desired ductility of EGC [46]. Moreover, PVA fibre can have a strong bonding with the matrix due to the presence of hydroxyl groups in its molecular chains [47], which has a higher tendency to rupture during the fibre pull-out and hence weaken the tensile ductility of the composites. Therefore, oil coating is normally adopted on the surface of the PVA fibre for reducing the probability of fibre rupture and achieving superior tensile ductility [48]. Polyethylene (PE) fibre with a hydrophobic surface feature was also often used to develop EGC with both high tensile strength and ductility. It is worth noting that the tensile strength of PE fibre (2700-3500 MPa) is higher than that of PVA fibre. Apart from PVA and PE fibres, polypropylene (PP), glass and steel fibres, chopped steel wool and multi-walled carbon nanotube (MWCNT) were also used for EGC. Although PVA and PE fibres are the most suitable reinforcements for EGC, their exceptional high costs and inevitable environmental impacts whilst the manufacture would result in lower cost-effectiveness and sustainability for EGC [49, 50]. As a result, recycled fibres from waste products including recycled tyre steel (RTS) and recycled tyre polymer (RTP) fibres have been employed to partially replace PVA fibres [51-53], which can not only be beneficial for the sustainability of EGC but also contribute to the reduction of solid wastes (waste tyres).

2.2. Manufacturing process

In general, EGC can be produced using either one-part or two-part mixing approach. Regarding the two-part mixing, the alkaline activator should be prepared separately before the mixing of EGC. For instance, blending NaOH and Na_2SiO_3 requires about 24 h to allow heat dissipation. It starts with the mixing of dry materials including precursors and aggregates (if any), followed by the addition of activators, water and additives (if any). Once the mixture reaches a flowable and consistent state, the fibres are gradually added to ensure uniform fibre distribution while avoiding fibre-clumping and fibre-balling. For one-part mixing, solid-state activators are mixed with the precursors and aggregates, and the remaining procedure is similar to that of two-part mixing. To improve the dispersion of some fibres (e.g., MWCNT), they are first mixed with dispersant and water [54]. It is worth noting that an effective dispersion of nanoparticles can be more conducive to improving the properties of the resultant composites [55]. There is no specific total time duration for the mixing of EGC as most studies used visual observation to define whether the consistent state of the paste (or mortar) samples was achieved. Regardless of the mixing approach, the total mixing time was in the range of 5-25 min.

The pouring method is the main approach to preparing EGC mixtures. As shown in Table 1, most FA-based EGC samples require heat curing (45-105 °C) to gain early-age strength while water curing at ambient temperature was typically adopted for GGBS-based EGC. EGC with a large proportion of GGBS may present poor workability, quick setting time and high shrinkage [56-59], which may not be favourable for engineering applications. To address the drawbacks of FA- and GGBS-based EGC, some researchers employed the blended FA and GGBS as the precursor of EGC and found that it can achieve desirable fresh properties and comparable or even better hardened properties to those with FA or GGBS under ambient temperature curing (around 20 °C) [12, 24, 52, 60-62].

3. Micromechanics-based design

3.1. Design theory

Unlike the design principle for high compressive strength in concrete (i.e., tight particle packing), the unique features of ECC or EGC are achieved using the micromechanics model that synergises the interaction between matrix, fibre, and fibre-matrix interface [1]. This design model is regarded as an effective tool to optimise the properties of ECC or EGC. To guarantee the strain-hardening and multiple cracking features for EGC, two criteria including strength-based and energy-based must be satisfied. Fig. 2a presents a typical tensile stress-crack opening response that will be used to explain how the above criteria can be fulfilled.

The strength-based criterion described in Eq. (1) stipulates that the cracking strength would not exceed the bridging capacity of fibres:

$$\sigma_{fc}, \sigma_c < \sigma_0 \tag{1}$$

where σ_{fc} is the stress required to initiate the first crack, σ_c is the stress required to form another crack (multiple cracks are formed already), and σ_0 is the maximum fibre bridging stress.

The cracking strength of EGC is normally influenced by the internal flaw size and K_m and would be dependent on the fibre bridging properties if the internal flaw is bridged by the fibre [1]. Herein, a higher K_m would result in larger cracking strength, which could increase the size of active flaw [1]. The active flaw means the flaw that can induce the new crack when the tensile stress is lower than the fibre bridging capacity [63]. Once the crack is formed, it will propagate along the weak zone, e.g., the interface between aggregate and cement paste [64]. Further, additional cracks will be initiated from the smaller size flaws as the tensile load increases. It should be noted that the localisation of fracture would happen if the tensile load required to generate a new crack from a flaw is higher than the bridging capacity of fibres at any of the formed multiple cracks [1].

Table 1 Summary of raw materials, mix design and curing regime collected from studies on EGC.

Ref.	Binder (weight ratio)	Activator	L/b (or W/s or W/b)	Additive (Add/b)	Aggregate		Fibre		Curing regime
					Type	Agg/b	Type (%, by volume)	Type (L_f/d_f, mm/μm) [strength, MPa]	
[45, 65]	GGBS (1.0)	$Ca(OH)_2$ + Na_2SO_4, $Ca(OH)_2$ + Na_2SiO_3	W/s (0.300-0.438)	SP (0-0.03) + VMA (0, 0.0016) + antifoamer (0-0.002)	Silica sand (100)[c]	0, 0.4	PVA (2.0), PE (1.75)	PVA (12/39) [1620], PE (18/12) [2700]	Water curing at 23 °C (26 d, 27 d)
[11]	FA (1.0)	NaOH (8)[a] + Na_2SiO_3 (2)[b]	L/b (0.45)	-	Sand (600, 1180)[d]	0.5, 0.75	PVA (0, 1.0, 2.0) + steel (0, 1.0, 2.0)	PVA (8/40) [1600], Steel (10/120) [2500]	60 °C (1 d) + air curing (27 d)
[66, 67]	FA (1.0)	NaOH + Na_2SiO_3 (3.2)[b]	L/b (0.4, 0.47)	-	Silica sand (110)[c]	0.3, 0.4	PVA (1.0, 1.5, 2.0)	PVA (12/39) [1620]	Air curing at 23 °C (27 d), 60 °C (4 h, 8 h, or 1 d) + air curing (27 d)
[68]	GGBS (0.6) + Cement (0.4)	$Ca(OH)_2$ + Na_2SO_4	W/s (0.4)	SP + methyl cellulose + defoamer (0.003)	Silica sand	0.4	PVA (2.0)	PVA (12/39) [1620]	Water curing at 23 °C (27 d)
[69-73]	GGBS (0.94, 1.0) + SF (0, 0.06)	$Ca(OH)_2$ + Na_2SO_4, $Ca(OH)_2$	W/s (0.21-0.45)	SP (0.0039-0.40) + VMA (0, 0.002, 0.01) + defoamer (0, 0.001, 0.1)	-	-	PVA (1.0, 1.3), PE (1.5, 1.75, 2.0)	PVA (8/40) [1600], PE (18/12, 12/16, 12/32) [2700, 3030]	Air curing at 23 °C (26 d), Water curing at 23 °C (1-88 d)
[12, 42, 62, 74-78]	FA (0.5, 1.0) + GGBS (0, 0.5) + GFS (0, 0.5)	NaOH (8)[a] + Na_2SiO_3 (2)[b], KOH (8)[a] + K_2SiO_3 (2.2)[b], $Ca(OH)_2$ + Na_2SiO_3 (2)[b], NaOH (8)[a], Na_2SiO_3 (anhydrous)	W/s (0.20, 0.23, 0.33), L/b (0.36, 0.45)	SP (0, 0.01)	Silica sand (165)[c] (212, 1180)[d], Expanded glass (125)[d], Ceramic microsphere (80)[c] (125)[d], Expanded perlite (43)[c]	0-0.6	PVA (2.0), PE (2.0)	PVA (8/39, 8/40) [1600], PE (12/12) [3500]	Water curing at 23 °C (27 d), 60 °C (1 d) + air curing (2 d)
[29, 30]	POFA (1.0)	NaOH (8)[a] + Na_2SiO_3 (3.3)[b]	L/b (0.50-0.65)	SP (0, 0.05, 0.10)	Dune sand	1.8	PVA (2.0)	PVA (8/40) [1600]	65 °C (1 d) + air curing at 25 °C (1-26 d)
[79]	FA (0.5) + GGBS (0.4) + SF (0.1)	K_2SiO_3 (1.25)[b]	L/b (0.37)	-	Silica sand (500)[d]	1.36	PVA (1.0, 2.0), Glass (1.0), Hooked-end steel (0, 1.0) + straight steel (0-3.0)	PVA (12/15) [1560], Straight steel (6/160, 13/160) [2250], Hooked-end steel (50/1000) [1150], Glass (13/130) [1620]	Air curing (3 d, 7 d, 28 d)
[27]	LS (1.0)	KOH (1)[a] + Na_2SiO_3 (3.5)[b]	L/b (0.7)	Borax (0.002)	Sand (1450)[c]	0.5	PP (2.0)	PP (12/20, 20/38) [220, 340]	Bagged-curing at ambient temperature (7 d, 28 d)
[80]	FA (0, 0.5) + GGBS (0.5, 1.0)	Na_2SiO_3 (anhydrous)	W/s (0.4)	-	Silica sand (212)[d]	0, 0.3	PE (0-2.0) + steel (0-2.0)	PE (13/17) [3000], Steel (13/180) [2850]	Water curing (27 d)
[81-83]	GGBS (1.0)	$Ca(OH)_2$, NaOH, Na_2SiO_3	W/s (0.3)	SP (0.001, 0.002, 0.003) + VMA (0.0004, 0.001)	-	-	PE (1.75)	PE (18/12) [2700]	Water curing at 23 °C (5 d, 26 d)

				+ anti-foaming agent (0.001)					
[84, 85]	FA (1.0)	NaOH (4-20)[a] + Na_2SiO_3	W/s (0.23)	-	Silica sand (710)[d]	0.3	PVA (2.0)	PVA (8/40, 12/40, 18/200, 24/200) [1600]	30-105 °C (1 d) + air curing (27 d), 60 °C (28 d)
[61, 86]	FA (0, 0.4, 1.0) + GGBS (0, 0.6, 1.0)	NaOH (8, 12)[a] + Na_2SiO_3 (2.0)[b]	L/b (0.60, 0.61, 0.63)	-	River sand	0.5, 1.0	PVA (1.0, 2.0, 3.0), Steel (1.0, 2.0, 3.0), PP (2.0, 3.0), Chopped steel wool (2.0, 3.0)	PVA (8/40, 13/100) [1100-1600], Steel (13/200) [2750], PP (12/50) [600-700], Chopped steel wool (2-6/20-60) [200-400]	Air curing (6 h) + 80 °C (4 h) + air curing (14 d), 23 °C and 95% RH (56 d) + 23 °C and 60% RH (14 d), 60 °C (1 h) + 80 °C (3 h) + 23 °C and 60% RH (70 d)
[87]	FA (0.7-1.0) + GGBS (0-0.3)	NaOH + Na_2SiO_3 (2.7)[b]	L/b (0.27)	-	-	-	PVA (2.0)	PVA (12/40) [1586]	50 °C (3 d, 7 d, 28 d)
[88, 89]	FA (0.97) + MK (0.03)	NaOH + Na_2SiO_3 (3.2, 3.3)[b]	L/b (0.53)	-	Silica sand (200)[d]	0.26, 0.3	PVA (1.5)	PVA (12/39) [1600]	80 °C (2 h) + 20 °C and 70% RH (2 d, 6 d, 27 d)
[24]	FA (0.7) + GGBS (0.3)	NaOH + Na_2SiO_3 (3.3)[b]	W/b (0.32)	-	-	-	PVA (2.0)	PVA (8/40) [1640]	20 °C and ≥ 98% RH (28 d)
[90]	FA (0.91-1.0) + Zeolite (0-0.09)	NaOH + Na_2SiO_3 (3.3)[b]	L/b (0.55)	-	Silica sand	0.3	PVA	PVA (12/39) [1600]	80 °C (2 h) + 20 °C and 70% RH (2 d, 6 d, 27 d)
[51, 60, 91]	FA (0.8) + GGBS (0.2)	NaOH (10)[a] + Na_2SiO_3 (2.0)[b]	L/b (0.4, 0.45)	SP (0.01)	Silica sand (130, 148)[c] (250)[d]	0.1-0.4	PVA (1.0, 1.5, 1.75, 2.0) + RTS (0, 0.25, 0.5)	PVA (12/40) [1600], RTS (20/150) [2850]	20 °C and 60% or 95% RH (6 d, 27 d)
[32]	GGBS (0.32-0.81) + SF (0.08-0.19) + IFA (0-0.6)	NaOH + Na_2SiO_3 (3.2)[b]	L/b (0.53)	-	Sand	0.26	PE	PE (12/24) [3000]	80 °C (2 h) + air curing (28 d)
[14, 92]	MK (1.0)	Na-alkali-based solution, K-alkali-based solution	-	-	Quartz sand (200)[d]	0, 0.5	PVA (2.0), PE (2.0)	PVA (12/40) [1600], PE (12/20) [2500]	Bagged-curing (14 d)
[54]	FA + GGBS + SF + MK	NaOH + Na_2SiO_3 (3)[b]	-	-	Silica sand	-	PVA (0.15, 0.2, 0.25) + MWCNT (0.05, 0.10, 0.15, by mass)	PVA (12/50) [1680], MWCNT (20-30/10-20) [-]	20 °C and ≥ 95% RH (27 d)
[28]	FA (0.23-0.30) + GGBS (0.52-0.70) + SS (0-0.25)	NaOH + Na_2SiO_3 (3.2)[b]	L/b (0.52)	-	Sand	0.3	PE	PE (12/24) [3000]	100 °C (2 h) + air curing (28 d)
[43]	GGBS (0.94, 1.0) + SF (0, 0.06)	$Ca(OH)_2$	W/s (0.18)	SP (0.03-0.06) + defoamer (0.001)	Crumb rubber	0, 0.06, 0.11	PE (1.75)	PE (18/12) [2700]	Water curing at 23 °C (26 d)
[93]	FA (0.1) + GGBS (0.9)	NaOH + Na_2SiO_3 (3.2)[b]	L/b (0.54)	-	Silica sand	0.3	PE (2.0)	PE (12/24) [3000]	80 °C (2 h) + 20 °C and 70% RH (0-119 d)

[94]	FA (1.0)	NaOH (7.2)[a] + sodium metasilicate pentahydrate powder	W/s (0.345)	SP (0-0.01) + VMA (0.001, 0.008) + defoamer (0.001, 0.0015)	-	-	PE (1.75)	PE (18/12) [2700]	80 °C (1.5 d) + 23 °C (21.5 d)
[13, 95]	MK (1.0)	NaOH (6-14)[a] + Na_2SiO_3	L/b (0.8)	-	Silica sand	0.4	PVA (2.0)	PVA (12/26) [1560]	20 °C and 95% RH (28 d)
[52, 53, 96]	FA (0.8) + GGBS (0.2)	NaOH (10)[a] + Na_2SiO_3 (3.15)[b]	L/b (0.45)	SP (0.01)	Silica sand (130)[c] (250)[d]	0.2	PVA (1.0, 1.5, 2.0) + RTP (0-1.0)	PVA (12/40) [1600], RTP (5.2/21.4) [761]	20 °C and 95% RH (27 d)
[31]	GGBS (0.73, 0.81) + SF (0.17, 0.19) + RM (0, 0.1)	NaOH + Na_2SiO_3 (3.2)[b]	L/b (0.53)	-	River sand	0.26	PE (1.9)	PE (12/24) [3000]	20 °C and 70% RH (27 d), 80 °C (2 h) + 20 °C and 70% RH (27 d)
[97]	FA (0.20, 0.40, 0.55) + GGBS (0.37, 0.60, 0.80) + SF (0, 0.08)	Na_2SiO_3 (anhydrous) + water glass	W/s (0.2)	Borax (0.051)	Silica sand (300)[d]	0.65	Steel (2.0, 3.0, 4.0)	Steel (13/200) [2000]	90 °C (3 d) + air curing at 23 °C (1 d)
[33, 34]	GGBS (0.97) + RHA (0.03)	NaOH (8)[a] + Na_2SiO_3 (2.22)[b]	W/s (0.3)	SP (0.07)	Silica sand, Silica sand + copper slag (2400)[d]	2.25-2.70	PVA (2.0)	PVA (6/39) [1604]	Air curing at 25 °C (3-90 d)
[35]	GGBS (0.5) + LCDG (0.5)	NaOH (4)[a] + Na_2SiO_3	W/b (0.35)	SP (0.02)	Silica sand (236.24)[c]	0-1.0	PE (2.0)	PE (12/20) [-]	Air curing (7 d) + water curing at 85 °C (1 d) + air curing (2 d)
[98]	FA (0.5) + GGBS (0.5)	Na_2SiO_3 (anhydrous)	L/b (0.52)	-	Silica sand (233)[c] (400)[d]	0.3-1.0	PE (1.5) + steel (0.5)	PE (18/17) [3000], Steel (13/200) [2850]	25 °C and ≥ 80% RH (28 d)
[99, 100]	FA (0, 0.5, 1.0) + GGBS (0, 0.5, 1.0)	NaOH (12)[a] + Na_2SiO_3 (3.1)	L/b (0.47)	SP (0.02-0.05)	Expanded glass	0.2	PVA (0, 1.0, 2.0) + PP (0, 1.0, 2.0)	PVA (12/39) [1620], PP (12/40) [450]	70 °C (1 d) + air curing (28 d)

Note: FA = fly ash, GGBS = ground granulated blast-furnace slag, SF = silica fume, MK = metakaolin, GFS = gypsum free slag, POFA = palm oil fuel ash, LS = ladle slag, SS = steel slag, IFA = incineration fly ash, RM = red mud, RHA = rice husk ash, LCDG = liquid crystal display glass, SP = superplasticiser; VMA = viscosity modifying admixture, PVA = polyvinyl alcohol, PE = polyethylene, PP = polypropylene, RTS = recycled tyre steel, RTP = recycled tyre polymer, MWCNT = multi-walled carbon nanotube, L/b = liquid-to-binder ratio (the mass ratio of total liquid over the mass of solid from the binder), W/s = water-to-solid ratio (the mass ratio of total water over the mass of solids from the binder and alkaline activator), W/b = water-to-binder ratio (the mass ratio of total water over the mass of solid from the binder), Add/b = additive-to-binder ratio, Agg/b = aggregate-to-binder ratio, L_f = length of fibre, d_f = diameter of fibre.

[a]: molarity of sodium or potassium hydroxide solution

[b]: silicate modulus of sodium or potassium silicate solution

[c]: average particle size, μm

[d]: maximum particle size, μm

The multiple cracking behaviour is strongly associated with fibre bridging [50]. The distinct difference between ordinary FRC and ECC in terms of the uniaxial tensile behaviour (see Fig. 1) lies in the different crack propagation modes. The crack propagation of normal FRC follows the Griffith crack propagation mode, where the crack opening increases indefinitely with crack length while the ambient load must be reduced to ensure equilibrium, leading to strain-softening behaviour [1]. By contrast, the flat crack propagation mode is normally observed in ECC or EGC, where the ambient load and the crack opening are maintained as constant as the indefinite extension of the crack length [1, 101]. To achieve such crack propagation mode, the following energy-based criterion must be fulfilled, i.e., the maximum complementary energy (J'_b) for fibre bridging must be greater than the energy consumed by fracturing the matrix (J_{tip}):

$$\begin{cases} J'_b \geq J_{tip} = \sigma_{ss}\delta_{ss} - \int_0^{\delta_{ss}} \sigma(\delta)\, d\delta = K_m^2/E_m \\ \sigma_0\delta_0 - \int_0^{\delta_0} \sigma(\delta)\, d\delta = J'_b \end{cases} \tag{2}$$

where δ_0 and δ_{ss} are the crack openings corresponding to the maximum fibre bridging stress (σ_0) and steady-state bridging stress (σ_{ss}), respectively, and E_m is the matrix elastic modulus.

To verify the criteria above, a series of experiments need to be performed to attain the fibre bridging stress-crack opening response (Fig. 2a), E_m and K_m. By conducting the uniaxial tensile test on the dog-bone shaped specimen with a notch around its middle part (Fig. 2b), the relation between fibre bridging stress and crack opening can be determined experimentally [102]. This relation can be computed theoretically by considering the two-way pull-out, matrix micro-spalling and Cook-Gordon effects, where the detailed computation procedure has been well summarised in Ref. [103]. A set of micromechanical parameters including fibre, matrix and fibre-matrix interface properties are required as inputs for the above theoretical analysis, most of which can be measured experimentally [103].

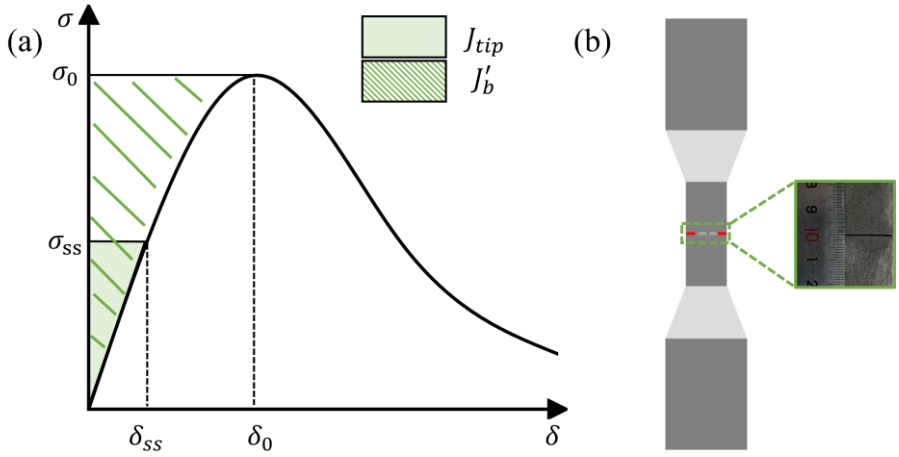

Fig. 2. (a) Typical relation between tensile stress and crack opening for fibre bridging [1] and (b) an example of the sample used for the single crack tension test (Note: σ_0 = maximum fibre bridging

stress, σ_{ss} = steady-state fibre bridging stress, δ_0 = crack opening corresponding to σ_0, δ_{ss} = crack opening corresponding to σ_{ss}, J_{tip} = crack tip toughness, J_b' = maximum complementary energy).

3.2. Fibre-matrix interaction

Based on Section 3.1, the tensile behaviour of EGC could be tailored by altering the properties of microstructural components (matrix, fibre and fibre-matrix interface). For instance, adjusting the fibre properties such as strength, elastic modulus and aspect ratio can vary σ_0 and J'_b [50]. The influences of various parameters on the properties of matrix and fibre-matrix interface which are closely associated with the tensile behaviour of EGC have been increasingly studied, as presented below.

3.2.1. Properties of matrix

As discussed previously, K_m is an important parameter for EGC and should be limited, which can be measured through a three-point bending test [1]. Fig. 3 shows some scatters of K_m and J_{tip} collected from the existing studies on EGC. In general, J_{tip} of most matrices rises with the increasing K_m. The measured K_m was in the range of 0.07-0.60 MPa·m$^{1/2}$, while the corresponding J_{tip} ranged from 0.57 to 65.80 Jm^{-2}. Most EGC matrices had smaller K_m values compared to the most commonly used M45 ECC (about 0.60 MPa·m$^{1/2}$ [7]), but higher J_{tip} values (around 15 Jm^{-2} [7]).

Regarding the effect of precursor, the presence of SS, zeolite or gypsum free slag (GFS) can significantly reduce K_m of the matrix without the above materials (15.91-68.18%) [12, 28, 90]. Nevertheless, the results from Ref. [28] contradicted Eq. (2), where J_{tip} of the matrix made from SS went up with the reducing K_m. Irrespective of sand addition, replacing GGBS with 50% FA led to an increased K_m [80], which was inconsistent with the effect of FA in ECC [7]. The lower reactivity of FA compared to GGBS could weaken K_m. Using 10% RM to replace GGBS and SF and rising the dosage of IFA (0-40%) increased K_m, while the presence of RM reduced J_{tip} under both ambient temperature and heat curing regimes [31, 32]. Differently, increasing the content of IFA from 0% to 10% resulted in a 29.27% rise in J_{tip}, while the further addition of IFA to 40% did not have a prominent influence.

K_m can be also affected by the type, dosage and properties of alkaline activator. By comparing four different activator types, the mixture activated by a combination of NaOH and Na_2SiO_3 had the highest K_m (0.436 MPa·m$^{1/2}$) and J_{tip} (22.4 Jm^{-2}), while both were the lowest when $Ca(OH)_2$ was used as the activator (0.086 MPa·m$^{1/2}$ and 4.1 Jm^{-2}) [77], which is consistent with the findings reported in Ref. [76]. Increasing W/s from 0.20 to 0.23 can effectively lower K_m and J_{tip} of EGC [74, 76]. As indicated in Ref. [24], both K_m and J_{tip} went up first when the silicate modulus of the activator changed from 0.8 to 1.0 and after which, they dropped, while adjusting the silicate modulus from 1.0-1.2 may lead to a different amount of reaction products along with disparate nature and thus different

values of K_m. Due to the higher compressive strength, the mixture with more sodium metasilicate pentahydrate powder exhibited a higher K_m and J_{tip} [94].

Independent of binder and sand types, the addition of sand considerably increased K_m and J_{tip} due to the increased energy consumption to propagate the crack [74, 80, 104, 105]. Both parameters were strongly sensitive to the sand size [74]. For instance, K_m and J_{tip} of mixtures containing coarse sand (1180 μm) were 6.22-17.82% and 23.18-29.68% lower than those of mixtures made of fine sand (212 μm) when a constant W/s was adopted. This was because the crack propagation path in the mixture containing coarse sand was less tortuous than that in the mix incorporating fine sand, consuming less energy [74]. There were no obvious changes in K_m and J_{tip} with curing age [89, 93]. Applying elevated temperature to cure the sample can reduce both K_m and J_{tip} as the microstructure of the matrix after ambient temperature curing was denser [12, 31].

In summary, K_m of EGC is highly related to its microstructure especially the amount and nature of reaction products. To attain superior tensile behaviour of EGC, K_m should be strictly controlled. There is a wide range of K_m for different types of EGC but a suitable range of K_m is required to define in future research, mainly considering the tensile behaviour.

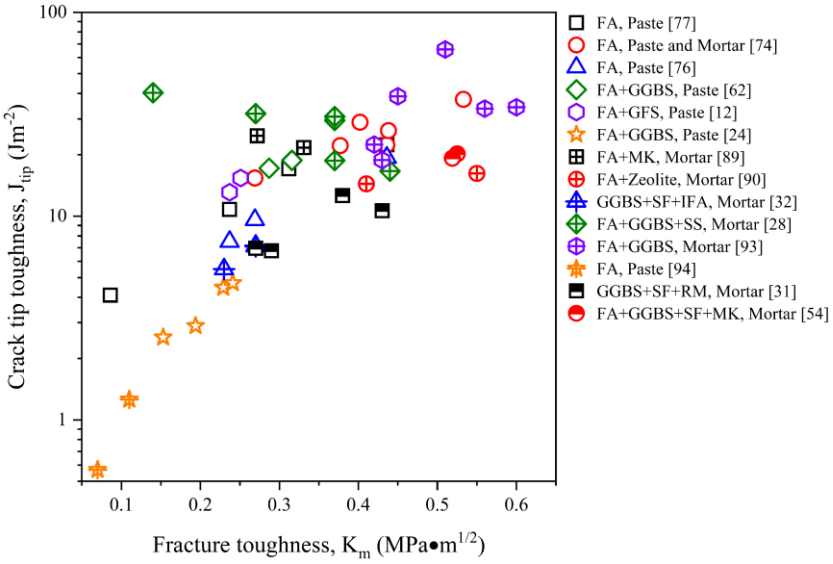

Fig. 3. Scatters of K_m and J_{tip} of EGC.

3.2.2. Properties of fibre-matrix interface

As aforementioned, the bridging fibres play an essential role after the crack initiation. As the crack propagates with the increasing crack opening, the bridging fibres de-bond and stretch across the crack interface until the complete pull-out or rupture [1]. This pull-out behaviour is associated with the fibre-matrix interface properties that can be measured by conducting a single fibre pull-out test (see Fig. 4a). A typical test curve in a single fibre pull-out test is illustrated in Fig. 4b, which can be mainly classified into two stages: (1) de-bonding, and (2) slippage/sliding [47]. To pull out a fibre (e.g., PVA), certain stress is first needed to overcome the chemical bond (G_d) to de-bond it, followed by

slippage/sliding depending on the frictional bond (τ_0) and slip-hardening coefficient (β). These three parameters can be evaluated as follows [47]:

$$\begin{cases} G_d = \dfrac{2(F_{pa} - F_{pb})^2}{\pi^2 E_f d_f^3} \\ \tau_0 = \dfrac{F_{pb}}{\pi d_f L_e} \\ \beta = \dfrac{d_f}{L_e}\left[\dfrac{1}{\pi \tau_0 d_f}\left(\dfrac{\Delta F_p}{\Delta S'}\right)|_{S' \to 0} + 1\right] \end{cases} \quad (3)$$

where F_{pa} is the maximum force when debonding length equals the embedment length of fibre, F_{pb} is the force at the start of fibre sliding, E_f and d_f are the elastic modulus and diameter of fibre, L_e is the embedment length, and S' is the sliding displacement.

Table 2 summarises the results of G_d, τ_0 and β obtained from the existing studies on EGC, considering the effects of supplementary materials (zeolite, IFA, GFS), activator (type, content, silicate modulus), W/s, fibre (type, aspect ratio), and curing condition. Regardless of fibre type, the measured G_d, τ_0 and β of EGC were in ranges of 0.46-6.10 Jm^{-2}, 0.55-6.53 MPa and -0.06-0.5, respectively. Compared to M45 ECC with PVA fibres [7], most EGC mixtures exhibited smaller G_d, τ_0 and β.

Unlike the influence on K_m, the inclusion of zeolite increased both G_d and τ_0 of EGC with no zeolite by 64.66% and 300.61% due to the facilitated reaction process caused by the zeolite [90]. The effects of GFS and IFA on the interface properties especially τ_0 and β followed the trend of K_m [12, 32], which can be attributed to the increased fracture surface toughness as a positive correlation was found between it and fracture toughness [106]. Hence, the contact areas between fibres and the matrix are increased, leading to a larger τ_0. Besides, a jamming effect can occur more easily because of the increased contact area and thereby a larger β. G_d is closely related to the type and composition of the reaction products attached to the surface of the fibre [7, 24].

Increasing W/s from 0.40 to 0.45 in GGBS-based EGC reduced G_d and τ_0 but did not change β [69], which agrees well with the findings for FA-based EGC when oil-coated PVA fibres were used [76]. Decreasing W/s would lead to fewer reaction products adhered to the fibre's surface and thereby lower G_d. By contrast, the oil-coating can weaken the jamming effect during the slippage and thus, β was insignificantly affected by adjusting W/s. However, τ_0 of FA-based EGC was found to rise by 33.08% when W/s was increased to 0.23, which is opposed to the observation in ECC that τ_0 dropped with the increasing water content [76]. The mixture activated by KOH and K_2SiO_3 exhibited a higher G_d but lower τ_0 and β compared to that using NaOH and Na_2SiO_3, where the higher G_d in EGC with K-based activator can be attributed to the loss of oil-coating agent on the PVA fibre's surface as a result of the higher alkalinity of KOH solution [76]. The changes in G_d and β with the silicate

modulus of the activator (0.8-1.5) followed the trend of K_m, while the tendency of τ_0 was different, which can be ascribed to the synergistic effect of fracture surface toughness and shrinkage-induced normal stress. Both τ_0 and β went up with the increasing dosage of sodium metasilicate pentahydrate powder, consistent with the trend of K_m [94].

By comparing PE fibre and PVA fibre, no chemical bond was observed for EGC with PE fibres and further, its τ_0 and β were 36.45% and 53.66% lower in comparison with PVA fibre reinforced EGC [62]. These reduced interface properties caused by PE fibre can be attributed to its hydrophobic feature. Similarly, as seen in Table 2, all PE fibre reinforced EGC did not have a G_d along with a slip-softening behaviour (β is less than 0). According to Ref. [107], τ_0 of EGC was reduced from 1.44 MPa to 0.82 MPa when the aspect ratio of used PE fibre declined from 1500 to 750 but remained constant when the aspect ratio further dropped to 375. Due to the denser microstructure, most ambient-cured EGC presented better interface properties than heat-cured EGC [12].

Regardless of reinforcing fibre type, the interface properties are associated with K_m, composition and amount of the reaction products on the fibre's surface, and shrinkage-induced normal stress, which should be adequate to promote complete fibre pull-out while avoiding fibre rupture. A few studies qualitatively correlate the interface properties with the tensile properties of EGC, which can help better tailor the tensile behaviour. More studies are required to consider other influencing parameters such as FA/GGBS ratio and fibre type to elucidate the links between them. Moreover, further research is needed to understand the effects of fibre embedment length and inclination angle of the fibre on the interface behaviour to get more insights into the fibre bridging mechanism.

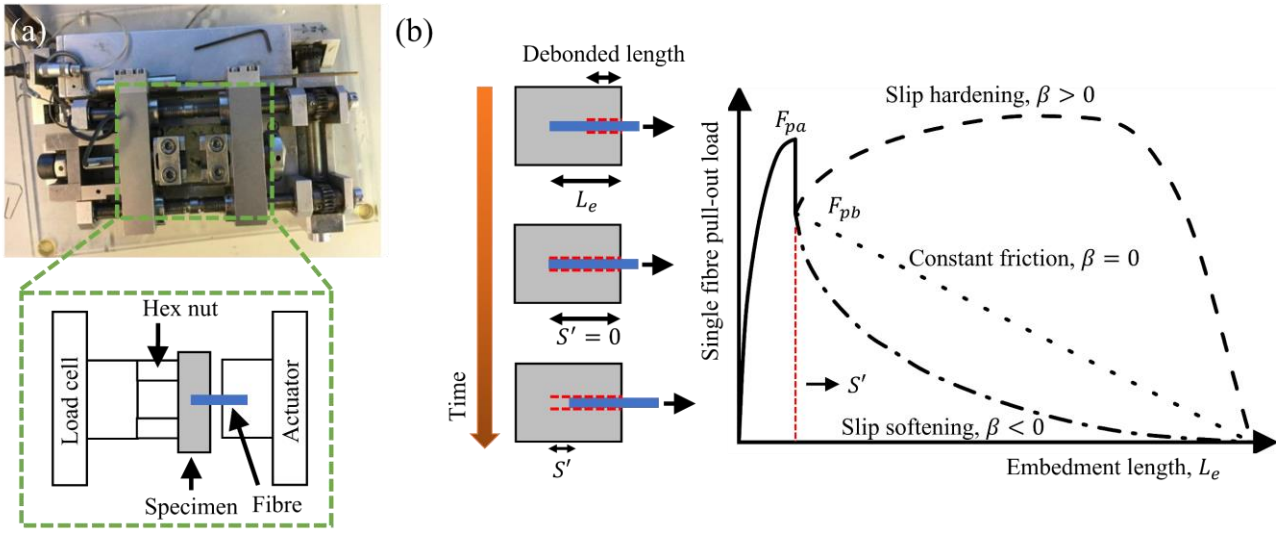

Fig. 4. (a) An example of a single fibre pull-out test setup, and (b) typical curves from single fibre pull-out tests [24, 47] (Note: F_{pa} = maximum force when debonding length equals the embedment length of fibre, F_{pb} = force at the start of fibre sliding, L_e = embedment length, β = slip-hardening coefficient, S'= sliding displacement).

Table 2 Summary of single fibre pull-out test results from existing studies.

Ref.	Binder	Fibre	Variable	G_d (Jm^{-2})	τ_0 (MPa)	β
[69]	GGBS (paste)	PVA	W/s (0.40, 0.45)	0.71, 1.13	1.14, 1.27	0.012
[75]	FA (paste)	PVA	-	1.31	1.3	0.499
[76]	FA (paste)	PVA	Activator type, W/s (0.20, 0.23)	0.59, 1.31, 3.41	0.87, 1.30, 1.73	0.03, 0.46, 0.50
[62]	FA + GGBS (paste)	PVA, PE	Fibre type, curing condition	1.03 (PVA)	1.32, 1.36, 2.14	0.014, 0.019, 0.041
[12]	FA + GGBS or GFS (paste)	PVA	Binder type, curing condition	0.46-1.03	1.14-2.14	0.021-0.049
[67]	FA (mortar)	PVA	-	6.1	0.7	0.33
[24]	FA+GGBS (paste)	PVA	Silicate modulus (0.8-1.5)	1.57-3.20	1.81-4.01	0.25-0.39
[90]	FA + Zeolite (mortar)	PVA	Zeolite content (0%, 6%)	1.16, 1.91	1.63, 6.53	-
[32]	GGBS + SF + IFA (mortar)	PE	IFA content (0%, 10%, 40%)	-	0.73, 0.95, 1.10	0.003, 0.004, 0.006
[72]	GGBS (paste)	PE	-	-	1.49	-0.06
[73]	GGBS (paste)	PE	Aspect ratio of fibre (375, 750, 1500)	-	0.818, 1.437	-0.0017, -0.0474
[94]	FA (paste)	PE	Activator content	-	0.55, 0.63	-0.0008, -0.0127

3.3. Strain-hardening indices

Both strength-based ($PSH_{strength}$) and energy-based (PSH_{energy}) indices can be used to quantify the possibility of achieving strain-hardening and multiple cracking behaviour for EGC. To attain a robust strain-hardening and saturated multiple cracking for ECC, $PSH_{strength}$ and PSH_{energy} should be higher than 1.2 and 2.7, respectively [108, 109]. These values were also used here as the requirements for defining the robust tensile behaviour of EGC. In general, $PSH_{strength}$ of most EGC ranged from 0.71 to 2.93, while PSH_{energy} was within 1.10 and 38.91. Most studies employed single crack tension tests (Fig. 2b) to estimate these index values [28, 31, 32, 52, 60, 93], while a few studies derived them from the theoretical relation between fibre bridging stress and crack opening [12, 24, 62]. Herein, only the studies that have determined both indices were discussed. Most mixtures can achieve a robust strain-hardening behaviour under uniaxial tension considering both indices, which were confirmed by the corresponding tensile stress-strain response and cracking patterns.

With the increase of IFA content from 0% to 10% and 40% in GGBS-SF based EGC, $PSH_{strength}$ was consistently increased, while PSH_{energy} went up first and then dropped [32]. The better PSH_{energy} can be ascribed to the higher σ_0 as a result of stronger τ_0. For all mixtures, both $PSH_{strength}$ (1.30-2.93) and PSH_{energy} (30.36-38.91) fulfilled the requirements of robust strain-hardening behaviour mentioned above for ECC. Moreover, the trend of tensile strength followed the

tendency of PSH_{energy}, while the trend of tensile strain capacity was consistent with that of $PSH_{strength}$. Under ambient temperature curing, no notable effects in $PSH_{strength}$ and PSH_{energy} were observed when 10% RM was adopted to replace GGBS and SF, while the mixtures containing RM had larger $PSH_{strength}$ and PSH_{energy} values (1.74 and 19.54) than those of EGC without RM (1.63 and 16.28) under heat curing [31]. These results were in good agreement with that for tensile properties. As mentioned in Section 3.2.1, the inclusion of SS led to increased J_{tip} and the calculated PSH_{energy} value was the lowest (6.58) at the highest SS substitution level [28]. Besides, the tensile properties were more sensitive to PSH_{energy}, instead of $PSH_{strength}$. Regardless of curing regime, EGC with FA and GFS exhibited lower $PSH_{strength}$ and PSH_{energy} values (1.10-1.11 and 1.73-2.07) than the mixes with FA and GGBS (1.42-1.44 and 2.09-2.38), indicating that the interface properties especially τ_0 and β played a more dominant role than K_m [12]. All studied mixes still presented conspicuous strain-hardening behaviour along with tensile strain capacity of 2.6-4.2% and reasonable variability although most of their indices were lower than those for ECC to achieve robust strain-hardening. The tensile properties of all mixtures were positively correlated with these indices. As seen in Fig. 5a, the use of activator with silicate modulus of 1.2 to fabricate EGC can lead to the highest $PSH_{strength}$ (2.63) compared to others with different silicate moduli, which can be attributed to the lower K_m and β as well as higher τ_0 [24]. However, both indices did not have a clear correlation with tensile properties.

As indicated in Fig. 5b, increasing the PVA fibre content (1.0-2.0%) can mostly improve the strain-hardening indices of FA-GGBS based EGC, while the increase of RTP fibre dosage (0.25-1.0%) consistently lowered them [52, 60]. The tensile strain capacity had a positive correlation with $PSH_{strength}$, whereas a slight inconsistency was captured for PSH_{energy}. Nevertheless, an opposite finding was reported in Ref. [60]. For the hybrid fibre reinforced EGC, only the mixture containing 1.75% PVA fibre and 0.25% RTP fibre can fulfil the requirements of robust strain-hardening stated for ECC. Because of lower τ_0 and β, PE fibre reinforced EGC exhibited higher index values than PVA fibre reinforced EGC under ambient temperature curing, consistent with the tensile strain capacity [62], due to the better fibre bridging behaviour as fewer fibres would undergo breaking or rupturing.

Regarding the influence of curing regime, it was revealed that heat-cured mixtures had higher strain-hardening indices than ambient-cured EGC [31, 62], which can be mainly attributed to the smaller K_m and J_{tip}. It should be noted that only the tensile strain capacity of these mixtures had a positive relation with the indices, while their tensile strengths exhibited opposite trends. A different conclusion was made in terms of the effect of curing condition, where ambient-cured EGC had a higher strain-hardening index than that with heat curing [12], as the strain-hardening indices can be

affected more significantly by τ_0 and β as compared to K_m. Both tensile strength and strain capacity showed a good correlation with $PSH_{strength}$ and PSH_{energy}. There was no clear trend in $PSH_{strength}$ of FA-GGBS based EGC when the curing period changed, while PSH_{energy} was consistently increased until 56 d [93]. The tensile properties were more sensitive to PSH_{energy}, where EGC achieved the highest tensile strength and strain capacity at 56 d.

In summary, the strain-hardening indices of most EGC had a positive relationship with their tensile properties. τ_0 and β can affect the strain-hardening indices more significantly as opposed to K_m and G_d. The index values for EGC to achieve a robust strain-hardening and saturated multiple cracking may be lower than those for ECC, which need to be confirmed with more data. Further work is required to establish the relationships between strain-hardening indices and tensile properties.

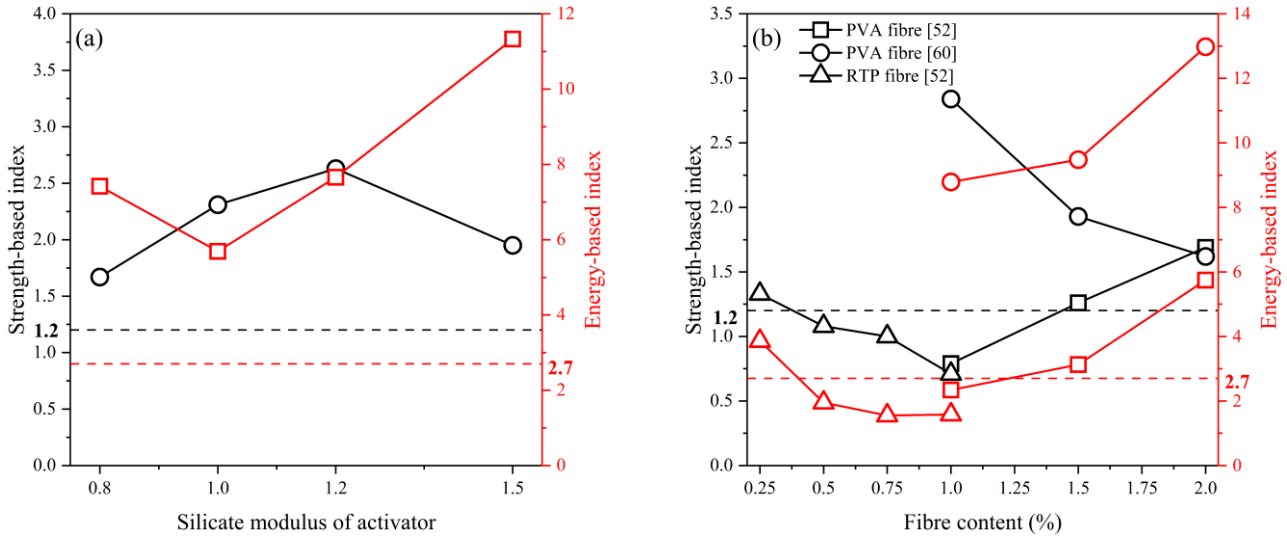

Fig. 5. Effects of (a) activator modulus [24] and (b) fibre content [52, 60] on strain-hardening indices of EGC.

4. Engineering properties

4.1. Workability

Workability is an important property for EGC, which was generally assessed using the flow table test [52, 60, 86]. Most available studies have focused on the effect of fibre in terms of type, content and aspect ratio on the workability of EGC, the results of which are shown in Fig. 6. Regardless of fibre type, a consistent trend can be found that increasing the fibre content can considerably decrease the slump flow of EGC, due to the reduced packing density and increased friction between fibres and between fibres and the matrix [110, 111]. A critical value exists for the fibre dosage and exceeding it can lead to a substantial reduction in workability and an increased possibility of fibre-balling or fibre-clumping, which is associated with the fibre aspect ratio [110]. The slump flow of EGC mixtures with PVA fibres with an aspect ratio of 200-300 was about 15% lower than that with a fibre aspect ratio of 90-120 since the higher aspect ratio of fibre may lead to more absorption of water or solution (larger fibre surface area) and increasing interaction with other solid particles and thereby impairing

the flowability [61, 85, 86]. Under the same Agg/b and molarity of NaOH solution, EGC with steel fibres presented higher flowability than that with PVA fibres [86], which can be ascribed to the strong hydrophilic feature of PVA fibres and smaller aspect ratio of steel fibres. Regarding the effect of fibre type, rigid fibres (e.g., steel) tend to raise the yield stress while flexible fibres (e.g., PVA, PP) typically increase the viscosity as they can be entangled as an S-shape structure to block the movement of particles [111, 112]. Apart from the mono-fibre reinforced EGC, some studies have investigated the influence of fibre hybridisation on the workability of EGC. Irrespective of binder type, using steel fibres to partially replace PE fibres resulted in better fluidity for EGC [80]. Utilising RTS fibres to substitute PVA fibres led to an 8.77-15.79% drop in slump flow compared to the mono-PVA fibre reinforced EGC [51]. This is because RTS fibres are less uniform in geometry and dimension than industrial steel fibres. The presence of 0.25% RTP fibre did not significantly vary the flowability of PVA fibre reinforced EGC, but further addition can weaken the slump flow due to the increased interaction between fibres with dissimilar shapes and properties [52].

Except for the fibre effect on the workability of EGC, a few studies explored the influence of parameters related to the matrix on the workability of EGC. Owing to the spherical shape and low reactivity of FA, the slump flow of FA-GGBS based EGC was higher than that prepared by GGBS only [61, 80, 99]. Increasing the molarity of NaOH solution from 8 M to 12 M caused an 8.11-27.59% reduction in slump flow of EGC [86], which can be attributed to the accelerated dissolution and polycondensation kinetics [113]. However, an opposite trend was reported in Ref. [29], which can be explained by the different nature of the precursor (FA against POFA). Similar to the effect of water-to-binder ratio (W/b) in cement-based materials, raising W/s from 0.40 to 0.45 improved the workability of EGC in terms of slump flow and V-funnel flow time [69]. Increasing Agg/b consistently decreased the workability of EGC due to the increased inter-particle friction and specific surface area [91, 98]. The increased specific surface area would require more paste to cover the aggregates. On the other hand, the particle packing can be enhanced with the increase of aggregate content and less paste would be required to fill the voids [114]. These two effects would compete simultaneously and the presence of a proper aggregate content would lead to better particle packing as well as acceptable workability for EGC. In addition, using 20% copper slag to replace silica sand was beneficial to the workability of EGC [33].

Controlling the viscosity of ECC's matrix can lead to a desirable fibre dispersion that can benefit the tensile behaviour [1]. The rheological behaviour of EGC is significantly disparate from that of ECC, which requires further research to understand the relationship between the matrix's rheology (especially yield stress and viscosity) and tensile properties of EGC as well as its fibre distribution. This can help achieve more robust tensile behaviour for EGC with less variation in material properties. Besides, for large-scale applications, an effective mixing protocol should be developed with specific

mixing equipment to improve the homogeneity of EGC and reduce the entrapped air voids caused by the high shear force and fibre.

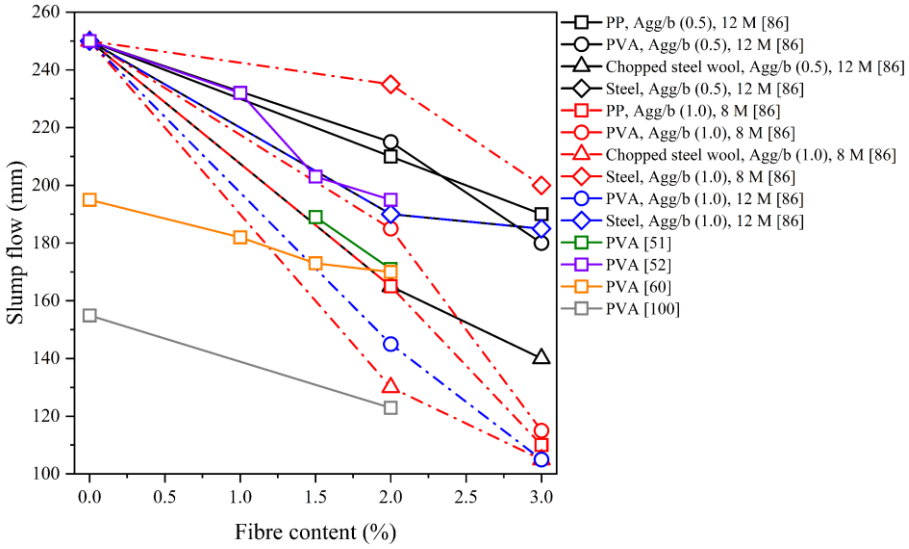

Fig. 6. Effects of fibre type and content on slump flow of EGC (Note: 8 M and 12 M denote the molarity of sodium hydroxide solution).

4.2. Setting time

Setting time is not a focus among the existing studies on EGC although it is crucial for engineering applications [115]. It was reported that the initial setting time and final setting time of GGBS-based EGC were only 25 min and 30 min, respectively, which were much lower compared with those of FA-based EGC (270 min and 300 min) [61]. Using blended FA and GGBS as the precursor can achieve an acceptable initial and final setting time for EGC (65-80 min and 90-110 min). By altering Agg/b of EGC (0-0.4), both initial and final setting time of FA-GGBS based EGC declined due to the decreased activator content [91]. Increasing the PVA fibre length from 8 mm to 13 mm did not significantly change the setting time of EGC [61], while raising either PVA or RTS fibre content shortened the setting time of EGC [51]. It should be noted that for conventional and some specific applications, the control of setting time is rather essential as it can affect the placing process as well as hardened properties [19].

4.3. Drying shrinkage

As mentioned earlier, coarse aggregates are normally eliminated from the mix design of both ECC and EGC, which could lead to a high drying shrinkage during the hardening process [116]. Further, several mix designs of EGC in Table 1 even did not include aggregates (i.e., pastes), making them more susceptible to shrinkage-induced cracking. Owing to the excellent shape stability of aggregates, the drying shrinkage resistance of EGC tends to be higher when the incorporated aggregate content is larger [91]. To date, very limited studies are available in terms of controlling the drying shrinkage of EGC, the results of which are presented in Fig. 7. Irrespective of fibre content, the drying shrinkage of PVA fibre reinforced EGC ranged from 3288 με to 13311 με at 28 d, which was much larger than

that of conventional ECC (1200-1500 με) [117]. It was found that using recycled fibres (i.e., RTS and RTP fibres) to partially replace PVA fibres can improve the drying shrinkage resistance of EGC [51, 52]. For instance, replacing PVA fibre with 0.5% RTS fibre in EGC led to a 72.63% drop in drying shrinkage at 28 d (1548 με) as compared with EGC with 2.0% PVA, which was comparable to traditional ECC. Besides the intrinsic properties of these recycled fibres, the improved shrinkage resistance caused by them can be associated with the reduced porosity and synergistic effect of hybrid fibres in controlling the cracks. However, some EGC mixtures with hybrid fibres still showed a large drying shrinkage as opposed to normal ECC, which may pose threats to their durability properties. To this end, further studies are required to find some effective approaches (e.g. using shrinkage-reducing admixture [118]) to reduce the drying shrinkage of EGC while maintaining other key engineering properties.

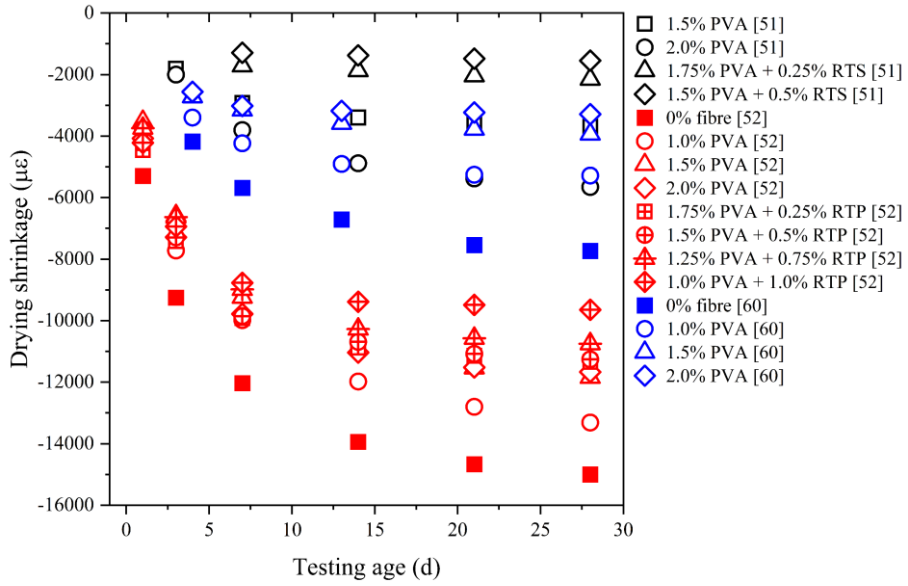

Fig. 7. Drying shrinkage of EGC with different fibre type and content.

4.4. Compressive behaviour

To date, there was about 36% of the mixes exhibiting a compressive strength between 10 MPa and 40 MPa. Although some of them have superior tensile behaviour, they can only be used for some non-structural applications due to their low compressive strengths [1]. Around 40% of them exhibited a compressive strength of 40-70 MPa, which is adequate for the requirements of most structural applications. Fig. 8 shows the effect of curing age on the compressive strength of EGC, indicating that regardless of binder and reinforcing fibre types, the compressive strength of EGC developed rapidly up to 28 d, after which the compressive strength was either increased slightly or even decreased [71, 89, 93]. The reduced compressive strength can be associated with the cracking induced by shrinkage. The highest compressive reached in EGC was 222 MPa but its tensile strain capacity was less than 0.4% [97]. As a promising EGC type, the highest compressive strength obtained in FA-GGBS based EGC was about 100 MPa at 28 d along with a tensile strength of 5.77 MPa and a tensile

strain capacity of 5.81% [93]. Only 28.5% of the EGC mixes had higher compressive strength than M45 ECC (about 68 MPa) [7].

The inclusion of some polymeric fibres such as PP and PVA fibres weakened the compressive strength of EGC although they resulted in substantial improvement in tensile strength [52, 60, 86]. Unlike steel fibres, the relatively lower stiffness of these polymeric fibres may entrap more air voids during the manufacturing process, resulting in higher local fractures near the fibres and thus diminishing the compressive strength [110]. Several studies on cementitious composites indicated that the presence of PVA fibres can result in higher porosity [119, 120]. Although the compressive strength of EGC was reduced after adding these fibres, the compressive ductility was enhanced along with higher integrity [52, 60].

Most of the existing studies have evaluated the compressive strength of EGC using samples with small sizes as per ASTM C109 [121], which is considerably smaller than most structural elements. Understanding the effect of sample size on the compressive strength of EGC would be valuable to justify whether the obtained results are valid for structural applications. The protocol for fibre addition is important as an inappropriate approach can induce many air voids inside the mixed sample, lowering its compressive strength. Therefore, this should combine with the suggestion mentioned in Section 4.1 to develop an effective protocol. For some specialised applications (e.g., impact and blast), it is essential to develop ambient-cured EGC with ultra-high strength (≥ 150 MPa) with superior tensile behaviour.

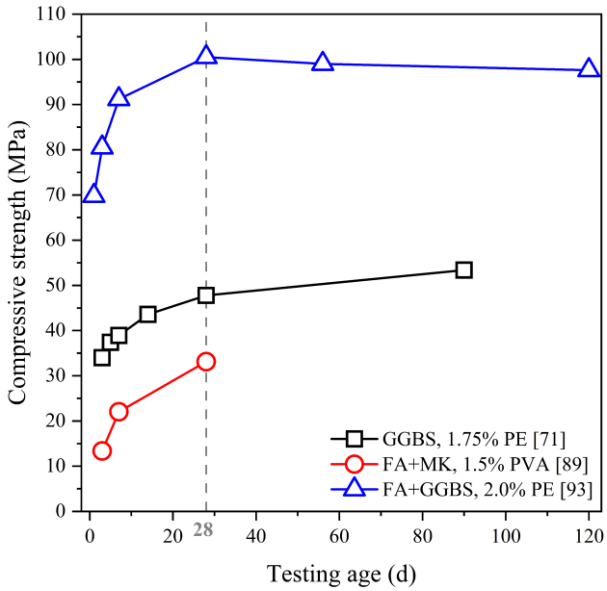

Fig. 8. Effect of curing age on compressive strength of EGC.

Besides compressive strength, elastic modulus is another important property for structural design. Fig. 9 shows the elastic modulus against compressive strength along with some existing equations for predicting the elastic modulus of Portland cement concrete [122, 123] and geopolymer concrete [124]. Similar to these equations, the elastic modulus of most EGC mixtures is positively correlated with

the compressive strength, while some conflicting results were reported that increasing Agg/b reduced the compressive strength of EGC but improved its elastic modulus [98], implying that the elastic modulus can be affected by aggregate more noticeably compared to compressive strength. The elastic modulus of EGC is also related to the properties of interfacial transition zone (ITZ) in EGC. It was found that an enhanced ITZ led to the improvement in elastic modulus of geopolymer concrete [59, 125]. Due to the absence of coarse aggregates, the elastic modulus of EGC that ranged from 0.8 GPa to 31.2 GPa was generally lower than that of normal and geopolymer concrete. The available data on EGC did not fit any of the existing models, and thus more data on elastic modulus for different compressive strength grades of EGC are required to develop a reliable model. Furthermore, no study can be found on Poisson's ratio of EGC, which needs to be estimated for potential applications.

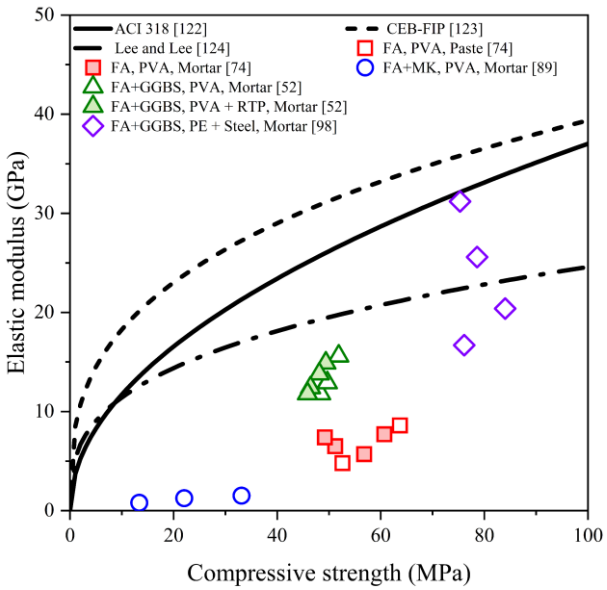

Fig. 9. Relation between elastic modulus and compressive strength for EGC.

4.5. Uniaxial tensile behaviour

Since uniaxial tensile behaviour is the most key property of EGC, many studies explored the effects of different factors on it in terms of stress-strain response, tensile strength and strain capacity, tensile strain energy, and fracture processes, which are comprehensively reviewed in this section.

4.5.1. Tensile stress-strain response

Similar to ECC, the tensile stress-strain response of EGC can be divided into three main regions: a linear elastic region, a strain-hardening region, and a strain-softening region. Some typical examples considering different factors are depicted in Fig. 10. The stress at the transition point between the linear elastic region and the strain-hardening region is called first cracking strength [80], while the highest point of stress is regarded as tensile strength and the corresponding strain is tensile strain capacity. Besides, the tensile strain energy known as strain energy density per unit volume can be used to reflect the strain-hardening degree of EGC, which can be determined by integrating the region of the tensile stress-strain curve prior to the strain-softening region [126]. As indicated, most EGC

mixtures from the existing studies can exhibit clear strain-hardening behaviour, while only a few of them presented pure strain-softening behaviour (e.g., those reinforced with low-strength fibres [86]).

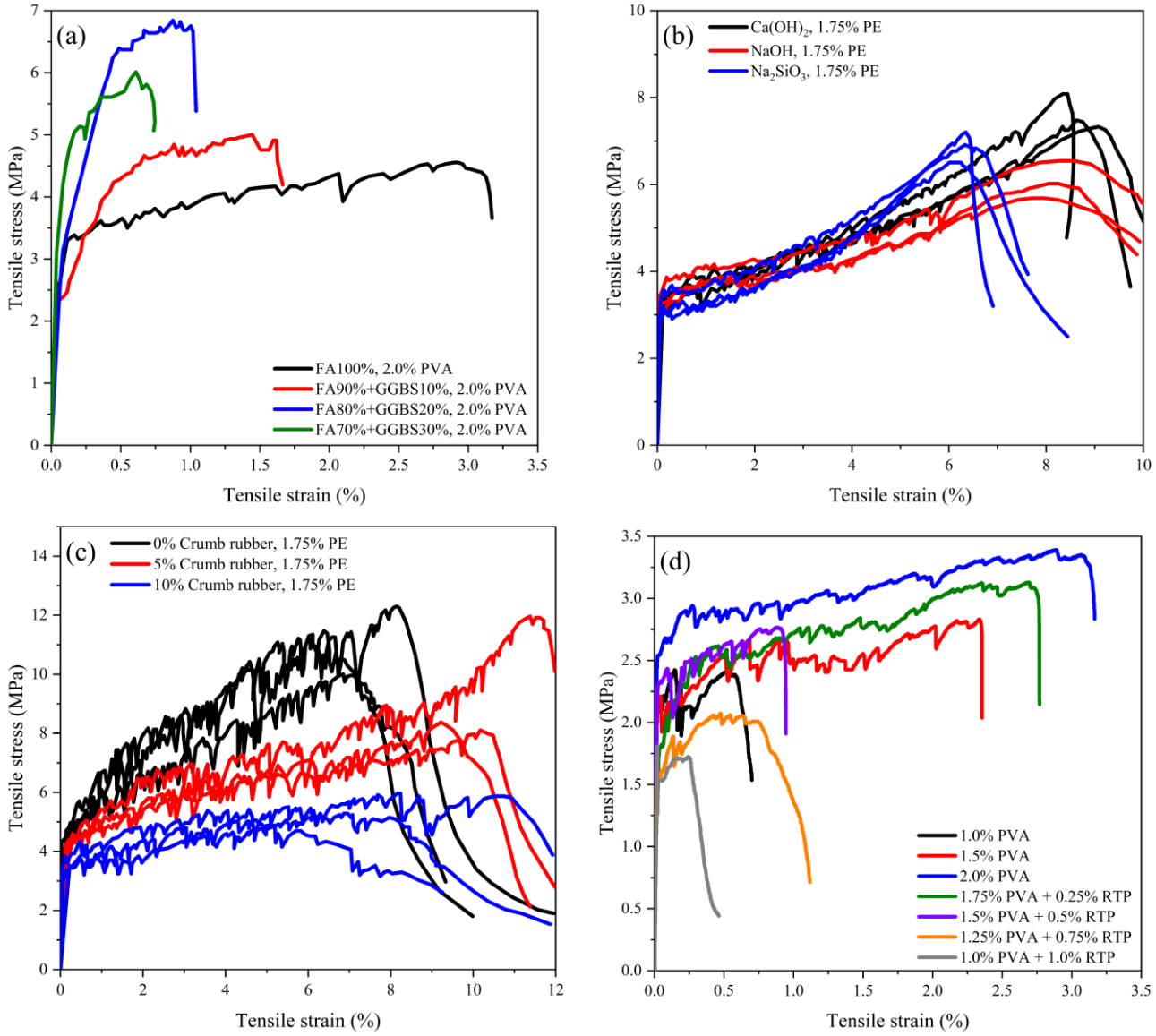

Fig. 10. Effects of (a) binder [87], (b) activator [83], (c) aggregate [43], and (d) fibre [52] on tensile stress-strain response of EGC.

4.5.2. Tensile strength and strain capacity

The available data on the first cracking strength is summarised in Fig. 11a, indicating that the first cracking strength generally rises with the increase of tensile strength. As mentioned previously, the first cracking strength of EGC is related to K_m and most studies affirmed it, where the first cracking strength of EGC tended to be larger at a higher K_m [12, 24, 31, 62, 74, 76, 80, 89, 94]. Nevertheless, some inconsistent results were also reported [32, 90, 93], since the inclusion of fibres can alter the internal pore structure of EGC and the first crack strength is also influenced by the pore size. In addition, the fibre bridging behaviour can influence the first cracking strength as some pores or flaws can be bridged by the fibres before tensile loading. This was confirmed by several studies that the mixtures containing fibres with different types or contents exhibited discrepant first cracking

strengths when they shared the same matrix [52, 60, 80]. Overall, it is important to understand the relationship between first cracking strength and pore structure (size and shape), where the pore structure can be characterised using advanced techniques, e.g., X-ray computed tomography [127]. Hence, a modified model based on the existing model of ECC [128] can be developed to better predict the first cracking strength of EGC.

The relationships between tensile strength and compressive strength as well as tensile strain capacity for EGC are shown in Fig. 11b and c, respectively, revealing that the tensile strength of most EGC rises with the increase of either compressive strength or tensile strain capacity (when the strain capacity is greater than 2%). In comparison with M45 ECC [7], about 27% of EGC mixtures exhibited a higher tensile strength ($>$ 4.86 MPa), while approximately 64% of mixes had a higher tensile strain capacity ($>$ 2.49%). As mentioned earlier, the tensile properties of EGC were strongly associated with the strain-hardening indices. To avoid replication, the studies discussed in Section 3.3 were not analysed here.

It was found that using 10-30% GGBS to partially replace FA improved the tensile strength of FA-based EGC by 8.51-44.68%, while the corresponding tensile strain capacity was 48.41-76.43% lower [87], which can be also reflected in Fig. 10a. The enhanced strength caused by the addition of GGBS was due to the increased amount of C-A-S-H and C-S-H gels, while the reduced strain capacity can be attributed to the lower stress index (i.e., ratio of tensile strength and first cracking strength). However, different results were found in another study that replacing 50% GGBS with FA impaired both tensile strength and strain capacity of EGC due to the smaller strain-hardening indices [80]. The addition of 3% and 6% zeolite can increase the tensile strength and strain capacity of FA-based EGC, whereas excessive addition of zeolite (9%) impaired them [90], due to the combined effect of increased τ_0 and reduced K_m after the presence of zeolite (see Section 3.2). With SF, the tensile strength and strain capacity of GGBS-based EGC were enhanced by 26.27% and 12.96%, respectively, owing to the increased packing density and densified microstructure [70].

Irrespective of the used matrix component, increasing W/s of EGC led to a reduced tensile strength and strain capacity, mainly due to the drop in fibre bridging capacity as a result of weaker interface properties [65, 69, 70, 74, 76]. The reduced fibre bridging capacity can be evidenced by the values of PSH_{energy}. Although rising W/s from 0.20 to 0.23 resulted in an improved τ_0 of EGC, its G_d was considerably weakened by 59.05%, which would accelerate the de-bonding process of fibres and in turn impair the fibre bridging effect [76]. Similarly, because of the better interface properties, the mixture made from NaOH and Na_2SiO_3 had the highest tensile strength and strain capacity of 4.7 MPa and 4.3% compared to those activated by NaOH, KOH and K_2SiO_3, and $Ca(OH)_2$ and Na_2SiO_3 [78]. 20% was regarded as the optimal content of sodium metasilicate pentahydrate powder considering the tensile properties of EGC [94]. As mentioned previously, increasing the content of

sodium metasilicate pentahydrate powder can induce better interface properties for EGC, while the excessive addition would impair the fibre bridging capacity as the extraordinary interface behaviour can increase the possibility of fibre rupture. The tensile properties can be also affected by the concentration of NaOH solution. Changing the molarity of NaOH solution from 8 M to 12 M did not lead to a significant variation in the tensile properties of FA-based EGC reinforced with both PVA and steel fibres [86]. However, a different finding was reported that increasing the molarity of NaOH solution up to 14 M resulted in a higher tensile strength of EGC due to the accelerated reaction process mentioned in Section 4.1 [95]. It should be noted that the tensile strain capacity dropped with the increase of NaOH concentration due to the decreased J_b' [95]. Additionally, the molarity of NaOH solution should be controlled as excessive OH^- would diminish the strength of EGC [85].

As stated earlier, the inclusion of aggregate is detrimental to the tensile strain capacity of EGC. As expected, independent of the used ingredient for the matrix, increasing the sand content generally increased the tensile strength of EGC but weakened the tensile strain capacity [35, 74, 80, 98]. For instance, raising Agg/b from 0.5 to 1.0 decreased the tensile strain capacity of PVA fibre reinforced EGC from 3.20% to 0.92% [86]. Although the matrix of EGC containing coarse sand had a lower K_m than that with fine sand (Section 3.2.1), the tensile properties were still about 22-64% smaller [74]. This can be ascribed to the poorer interface properties when coarser sand was used. To enhance the sustainability of EGC, other types of aggregates were adopted to replace the commonly used sand partially or fully. By incorporating expanded glass, ceramic microsphere and expanded perlite as aggregates in EGC, both tensile strength and strain capacity of EGC were not improved as compared to the mixture prepared with silica sand [42]. Applying 40% copper slag to replace silica sand led to a 45.52% and 59.38% rise in the tensile strength and strain capacity of EGC, respectively [34]. Crumb rubber was also added into EGC as aggregate to reduce K_m, which can improve the multiple cracking behaviour via introducing more active flaws [1]. As shown in Fig. 10c, the presence of a certain content of crumb rubber can lead to better tensile strain capacity while maintaining adequate tensile strength for EGC [43].

As aforementioned, defoamers were used to avoid the formation of unintentional large pores whilst the manufacturing process and the effect of their contents was presented in Ref. [45], indicating that the addition of 1% and 2% defoamer can increase the tensile strength and tensile strain capacity of EGC by 26.12-27.27% and 11.15-23.16%, respectively. Normally, the reduced porosity induced by the use of a defoamer could improve K_m and thereby weakening the tensile strain capacity. However, the defoamer would result in increasing interface properties and thus better fibre bridging behaviour as well as higher strain capacity. This is consistent with the previous discussion in Section 3.3 that the interface behaviour can affect the strain-hardening indices more significantly compared to K_m.

Irrespective of fibre type, several studies illustrated that increasing the fibre content consistently improved the tensile properties of EGC [27, 52, 79, 86], while some indicated that there was a limit for PVA fibre content (1.5%) since over which, the tensile properties were not enhanced [60, 67]. Although other types of fibre were also used to fabricate EGC, the resultant tensile strain capacity was typically less than 0.5%, as demonstrated in Fig. 11c [80, 86, 97]. The unimproved tensile strain capacity was mainly due to insufficient fibre bridging behaviour. For instance, the number of steel fibres crossing a certain area is significantly lower compared to that of PVA fibres due to the larger diameter of steel fibres, reducing the fibre bridging efficiency. Nevertheless, the tensile strength of steel fibre reinforced EGC was 10.84-88.49% higher than that of PVA or PE fibre reinforced EGC [80, 86]. Regardless of binder type, partial replacement of PE fibres with steel fibres up to 0.5% was feasible to maintain the acceptable tensile behaviour for EGC [80]. The aspect ratio of the fibre can also affect the tensile properties of EGC, where the mixtures possessed higher tensile properties when the reinforcing fibre had a higher aspect ratio [61, 73, 85], which can be mainly ascribed to the better fibre bridging stress when the fibre has a higher aspect ratio.

It was noticed that heat curing impaired the tensile strength of EGC but improved its tensile strain capacity due to the existence of more flaws induced by shrinkage cracking [61], while it was observed that both tensile parameters of FA-based EGC were improved when heat curing was used [66]. Regarding the effect of the curing time, the tensile strength and strain capacity of GGBS-based EGC were found to stop rising after 7 d [71], which can be attributed to the high reactivity of GGBS in the early ages. Differently, increasing the curing period from 3 d to 7 d and 28 d, the tensile strength of FA-MK based EGC did not change considerably, while its tensile strain capacity was decreased by 5.88% and 23.53%, respectively [89]. The different trends for these two EGC types can be explained by their disparate reaction mechanism and products.

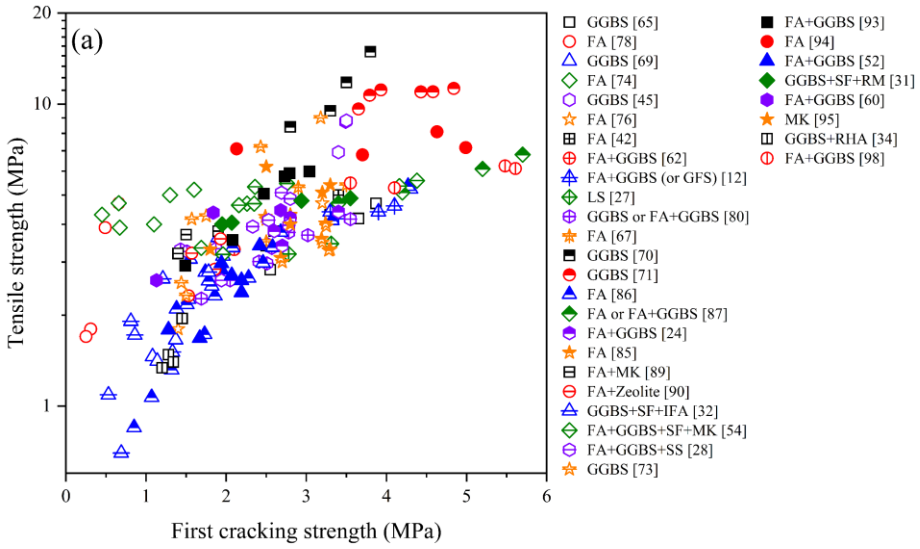

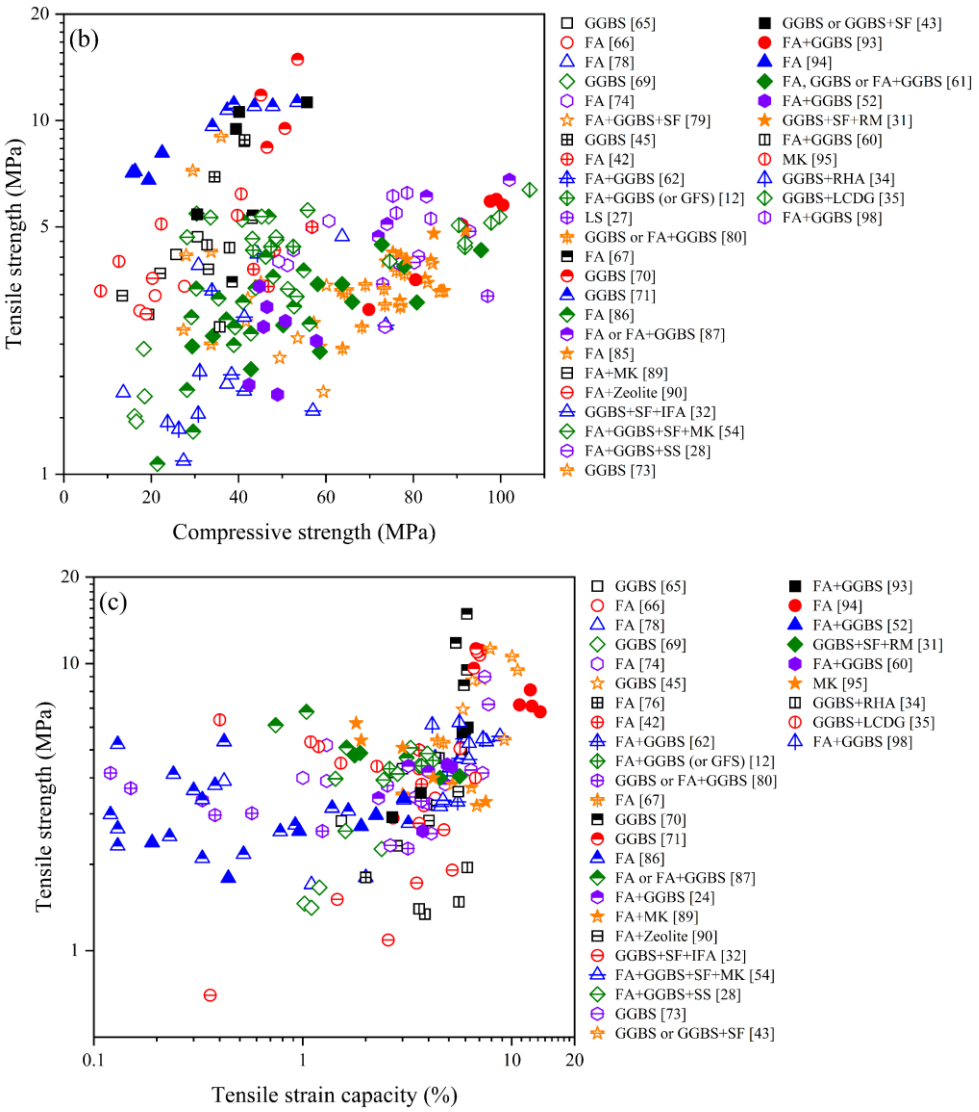

Fig. 11. Relations between tensile strength and (a) first cracking strength, (b) compressive strength and (c) tensile strain capacity for EGC.

Fig. 12 illustrates the fibre bridging behaviour of EGC under uniaxial tension. Given that the pre-existing pore is not bridged by the fibre (see the microscopic image), the first crack typically initiates from the largest pore inside the specimen. As the tensile load increases, the crack would propagate along the weakest zone (e.g., interface between paste and aggregate) and the fibres at the interface start bridging it. It should be noted that fibres are regarded as 2D randomly distributed inside the dog-bone shaped specimen [129], which can have different embedment lengths and inclination angles. The complete fibre pull-out behaviour would contribute to the improved fibre bridging capacity while ruptured fibres can impair it. For the identical matrix, the interface properties are comparable while the different fibre failure modes can be caused by the distinct embedment lengths and more importantly the disparate inclination angles. Besides, if the interface properties are too high, the fibres would be more easily damaged when passing through the rough matrix and thus causing the fibre rupture [1]. At the cracking interface, the fibres with longer embedment lengths can improve the fibre bridging behaviour given that the length is lower than the critical value [130]. However, the fibres

with higher inclination angles would impair the fibre bridging performance since they tend to rupture as a result of reduced fibre strength. The reduction in fibre strength is induced by fibre surface abrasion, local bending and lateral stress [131]. Further, the matrix spalling may happen at the exit point, which reduces the effective embedment length and thus diminishes the pull-out resistance [1].

Overall, it was suggested that changing the same parameter does not lead to a consistent tendency in tensile behaviour for EGC made up of different constituents, which can be attributed to the difference in the microstructure. Additional work is urgently needed to estimate the tensile properties of EGC in relation to microstructure (especially pore structure) and fibre distribution (orientation coefficient and inclination angle). The microstructure and properties of ITZ in EGC should be explored to gain more insights into the tensile behaviour. It was reported the properties of ITZ in geopolymer concrete can be affected by the mix proportions and boundary regions [132-134]. Besides, for structural purposes, the size effect on the tensile properties of EGC should be explored.

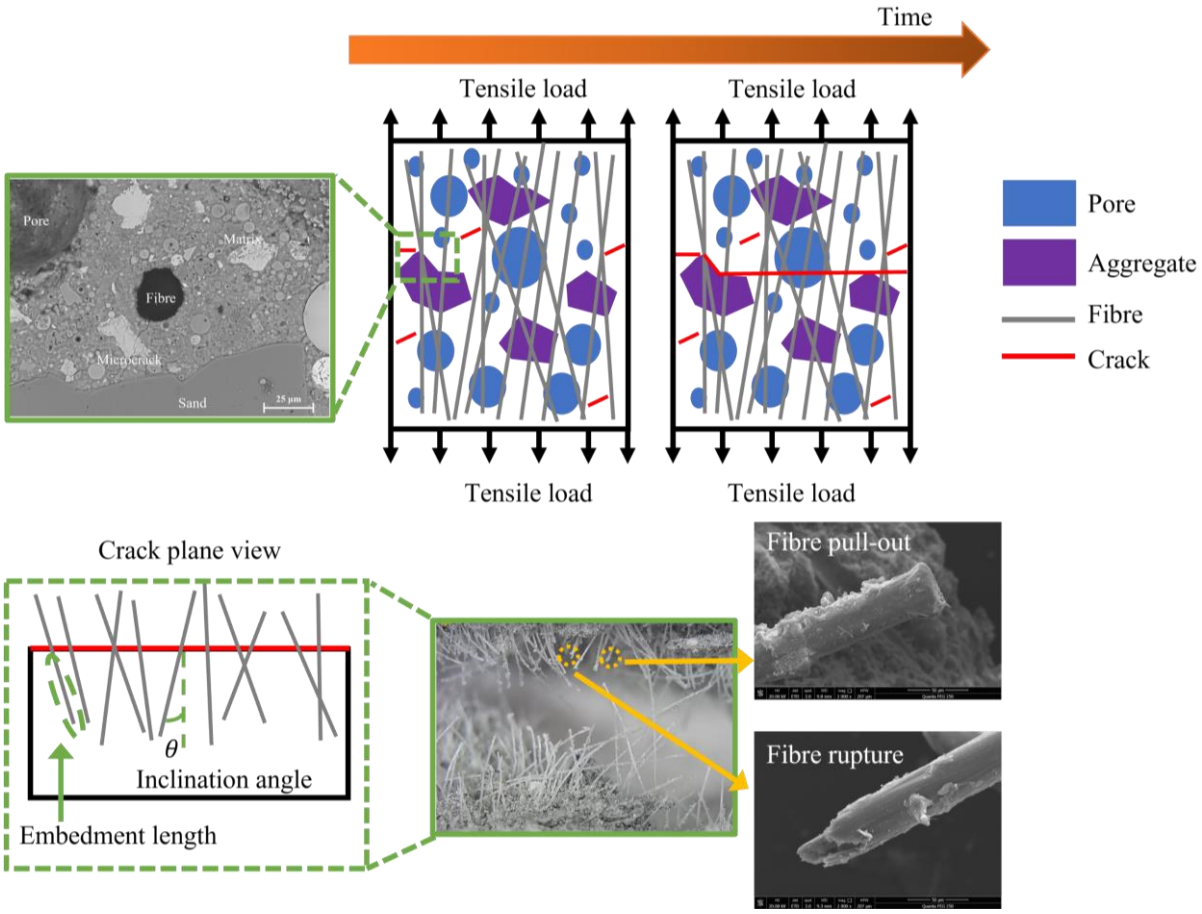

Fig. 12. Schematic diagram of fibre bridging action of EGC under uniaxial tension [52, 130].

4.5.3. Tensile strain energy

Fig. 13 summarises the available results on the tensile strain energy of EGC. As expected, the tensile strain energy improves with the increase of tensile strain capacity. In other words, the higher the tensile strain energy, the stronger the strain-hardening performance. Specifically, the tensile strain energy of EGC ranged from 0.18 kJm^{-3} to 780 kJm^{-3}, where the highest one was about 5.3 times

higher than that of normal ECC [135]. It should be mentioned that EGC mixtures that can achieve tensile strain energy of over 300 kJm^{-3} are mostly made from GGBS, while there was one produced with FA. However, as mentioned in Section 2.2, some drawbacks existed for these types of EGC and FA-GGBS based EGC holds promises to address those deficiencies. As seen in Fig. 13, only one study has examined the tensile strain energy of FA-GGBS based EGC, and more studies on other FA-GGBS based EGC in this aspect are needed. In addition, the tensile strain energy can only reflect the energy absorption capacity of EGC during the linear elastic and strain-hardening regions, which is not enough for the analysis of PE fibre reinforced EGC. Unlike PVA fibre reinforced EGC (Fig. 10a and d), a pronounced strain-softening region exists for EGC with PE fibres (Fig. 10b and c). To fully understand the energy dissipation characteristics of PE fibre reinforced EGC, the dissipated energy during the strain-softening region should not be ignored [136].

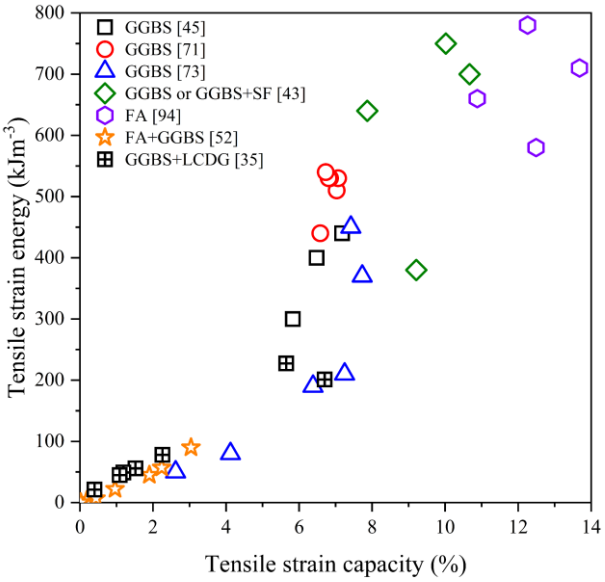

Fig. 13. Relation between tensile strain capacity and tensile strain energy for EGC.

4.5.4. Cracking analysis

Analysing the cracking characterises of EGC can help understand its crack-controlling performance. Fig. 14 gives an example of the damage evolution in EGC under tensile loading, indicating that the number of cracks raised with the increasing tensile load along with the reduced crack spacing [66]. This section will mainly focus on the crack spacing and crack width of EGC.

The relation between crack spacing and tensile strain capacity of EGC is presented in Fig. 15a, where most results of crack spacing were evaluated by dividing the gauge length (typically 80 mm for a dog-bone shaped specimen) by the number of cracks [28]. A prominent trend can be found that the higher the tensile strain capacity, the lower the crack spacing. The range of crack spacing for EGC was wide, from only 0.56 mm to 29 mm. Mostly, the crack spacing was lower than 8.6 mm when the tensile strain capacity was higher than 2%.

Fig. 15b shows the relationship between crack width and tensile strain capacity of EGC. Herein, 'R' means the residual crack width, which can be measured using a digital microscope. 'L' denotes the crack width mainly determined by dividing the highest tensile deformation by the number of cracks [28]. Both methods can be regarded as indirect approaches to assessing the crack width of EGC and the obtained results would be smaller than those under the actual loading [104]. Generally, it can be found that irrespective of residual or loaded crack width, the crack width tends to reduce with the increase of tensile strain capacity. Nevertheless, there was no significant change in crack width at a higher tensile strain capacity (over 10%) [94]. The crack width of EGC was in the range of 20.2-379.9 μm, and more than 71% of the results were less than 100 μm which was similar to the crack width of a typical ECC [104]. These tight crack widths can offer benefits to self-healing and durability of EGC [137], which will be discussed in Sections 4.9 and 5.

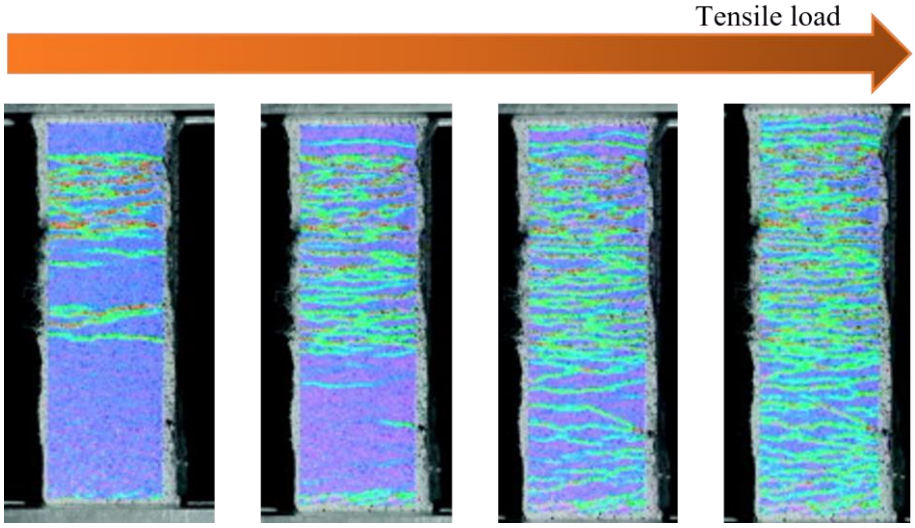

Fig. 14. Microcrack development in EGC with the increase of tensile load [66].

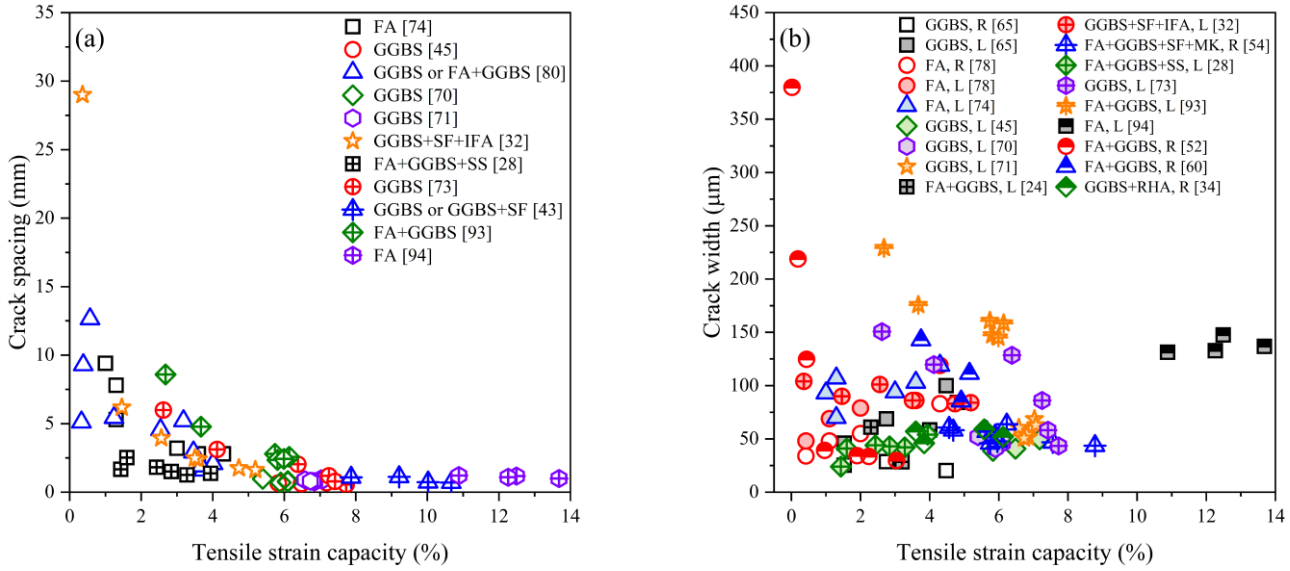

Fig. 15. Relations between tensile strain capacity and (a) crack spacing and (b) crack width for EGC (Note: R = residual crack width, L = loaded crack width).

4.6. Flexural behaviour

As seen in Fig. 16, in addition to deflection-hardening behaviour, multiple cracking can be observed for EGC. Under flexural loading, a crack can be induced locally at the weakest zone, while the fibres at the interface bridge it, sustaining and transferring the stress. Whist the crack opens continuously, and the fibres undergo the pull-out process, additional microcracks would be generated. Similar to uniaxial tension, fibre pull-out is favourable for improving the strain-hardening behaviour whereas fibre rupture can weaken it. Until now, limited studies have characterised the flexural strength of EGC using the four-point bending test, the results of which are presented in Fig. 17. A general trend can be observed that the flexural strength grows with compressive strength, ranging from approximately 4 MPa to 33 MPa. The flexural behaviour of EGC can be influenced by the aggregate size and content, NaOH concentration and more importantly, fibre type and dosage. Most of the studied mixtures can possess a pronounced deflection-hardening feature.

The changing trend of flexural strength with the molarity of NaOH solution (6-14 M) was consistent with that of compressive strength, where the highest flexural strength was attained when the used molarity was 12 M [13]. Nevertheless, the ultimate deflection of EGC was generally reduced with the increasing NaOH concentration, which can be ascribed to the increased K_m, similar to the reason for the reduced tensile strain capacity [95].

The inclusion of silica sand improved the flexural strength, deflection and toughness of EGC by 16.51-38.43%, 2.48-13.06% and 43.75-93.75%, respectively, and the optimal Agg/b was found to be 0.2 [91]. Similar results were reported in Ref. [11] that the flexural strengths of EGC with steel or PVA fibres were enhanced by 30.83% and 6.87% respectively when the content of sand with a smaller size (0.6 mm) increased from 0.5 to 0.75, while no improvement was found when the used sand had a larger size (1.18 mm). There was no clear trend in terms of flexural deflection and toughness when either sand size or sand content changed. Like compressive and tensile strengths, using 40% copper slag to replace silica sand resulted in the highest flexural strength for EGC, mainly due to the formation of ferrosialates induced by the reaction between alkaline activator and iron oxide from the copper slag [34].

Due to the higher stiffness of steel fibres, the mixtures with steel fibres outperformed the PVA fibre reinforced mixtures in terms of flexural strength (50.88-98.05% higher) [11]. While the low stiffness of PVA fibres was more beneficial for the flexural deflection of EGC. The mixtures with hybrid steel and PVA fibres (1.0% + 1.0%) exhibited lower flexural strengths than steel fibre reinforced EGC but higher compared to PVA fibre reinforced EGC. However, opposite results were also reported in terms of the flexural properties of EGC with steel or PVA fibres [79]. Replacing 0.25-0.5% PVA fibre with RTS fibres did not improve the flexural strength and deflection of PVA fibre reinforced EGC, while their flexural toughness was comparable [51], which can be ascribed to the

irregular geometrical characteristics of RTS fibres, similar to that contributing to the reduced workability (Section 4.1).

It is worth mentioning that the mixture showing deflection-hardening behaviour may not mean it would possess strain-hardening behaviour under uniaxial tension [1] and therefore, very limited studies have conducted the bending test to investigate the tensile behaviour of EGC. Further research can be concentrated on the strengthening performance of reinforced concrete beams with EGC.

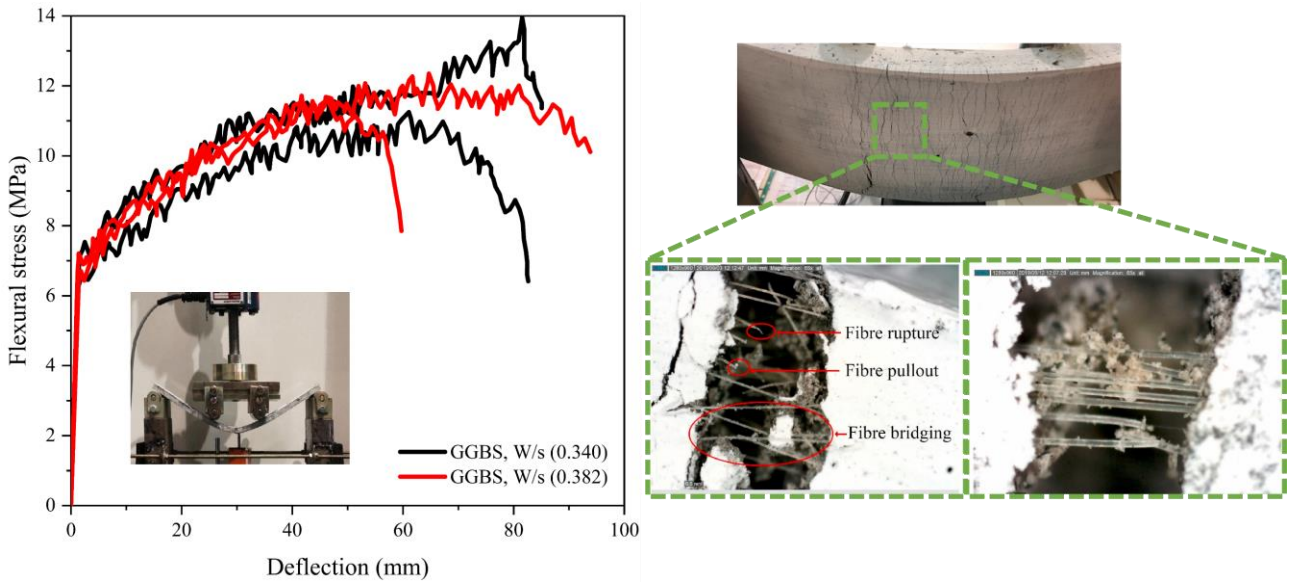

Fig. 16. Typical flexural behaviour and failure mode of EGC [65, 91].

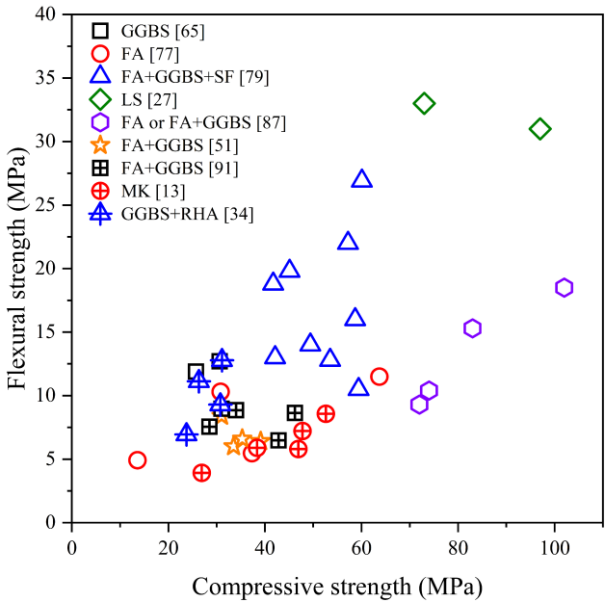

Fig. 17. Relation between flexural strength and compressive strength for EGC.

4.7. Dynamic mechanical behaviour

Traditional reinforced concrete structures may be susceptible to various extreme loading conditions (e.g., impact and blast) owing to the brittleness of plain concrete as well as its weak energy absorption capacity [138]. As shown in Fig. 18, these extreme conditions have higher strain rates ranging from 10^{-1} to 10^{3} s^{-1} and are dynamic, while the mechanical properties discussed in the last several sections

belong to quasi-static loading regimes. To improve the resistance of concrete structures against various extreme loading conditions, utilising EGC as part of these structures is a promising option.

To date, only a very few studies have examined the dynamic mechanical properties of EGC and various test methods were employed including direct tensile test [61], low-velocity drop weight test [13, 95], split Hopkinson tension bar test [14], and split Hopkinson pressure bar test [53, 60]. The strain rate that can be achieved during the direct tensile test is normally less than 1 s^{-1} [61], while using the latter two can get higher strain rates (over 10 s^{-1}) [138]. Similar to ordinary concrete, a remarkable strain rate effect can be observed in EGC that both dynamic compressive and tensile strengths went up with the rising strain rate (see Fig. 19) [53, 60, 61]. This can be attributed to the generation of more cracks caused by the insufficient time for crack propagation, the Stefan effect induced by the viscosity of free water and some structural effects (i.e., lateral inertia and end friction confinement) [139-141]. A parameter called dynamic increase factor can be used to quantify it. However, the tensile ductility exhibited a downward trend with the increase of strain rate, which can be ascribed to the increased interface properties especially G_d [1, 14, 61]. Thus, more fibres may be ruptured, leading to reduced fibre bridging behaviour and thereby the ductility is weakened. Such explanation is not valid for all studied EGC mixtures as one study observed more pulled out PVA fibres under dynamic loading due to improved fibre properties [14]. Besides the fibre and interface properties, the fibre embedment length and inclination angle can also affect the fibre failure mode. Given the reduced ductility, most EGC mixtures lost their strain-hardening and multiple cracking features under dynamic tensile loading and even some mixes showed a single crack localisation.

Apart from the strain rate effect, the dynamic mechanical properties of EGC can be also affected by the matrix composition, fibre and curing regime. Regardless of curing condition, the dynamic tensile strength of FA-GGBS based EGC was higher than that of FA- and GGBS-based EGC at a strain rate of around 0.5 s^{-1} [61]. Similar to the quasi-static mechanical properties, increasing the fibre aspect ratio from 130 to 200 resulted in a 7.03-36.75% rise in the dynamic tensile strength of EGC. Given that heat curing can induce more shrinkage cracks, most heat-cured EGC exhibited a higher tensile strain capacity but lower tensile strength than ambient-cured EGC under dynamic loading. Besides, all EGC with heat curing exhibited ductile failure rather than brittle failure as observed in most ambient-cured EGC. The strain at fracture localisation of EGC with PE fibres was about 44% larger than that of PVA fibre reinforced EGC at a strain rate of about 300 s^{-1}, which can be ascribed to the higher crack density [14]. This can be also explained by their bond strengths under dynamic loading. As aforementioned, the interface properties especially G_d of EGC with PVA fibres can be enhanced with the increasing strain rate, which would impair the bond strength. By contrast, only τ_0 of PE fibre reinforced EGC would be improved as it does not possess G_d, which is beneficial to the bond strength. These can be supported by Fig. 20 that more residual particles remained on the surfaces

of PVA fibres while no obvious attached particles can be observed for PE fibres. Owing to the smaller diameter and larger collective embedment surface of PE fibres, EGC with PE fibres should exhibit a higher dynamic tensile strength than PVA fibre reinforced EGC. Nevertheless, the experimental results in Ref. [14] did not illustrate such phenomenon, which could be associated with the dynamic tensile strength of PE fibres. Based on the impact performance of EGC after subjecting to a drooping hammer with various heights (100-800 mm), it was found that the threshold NaOH molarity for EGC was 12 M as the impact energy dropped when the used NaOH molarity altered from 12 M to 14 M [95].

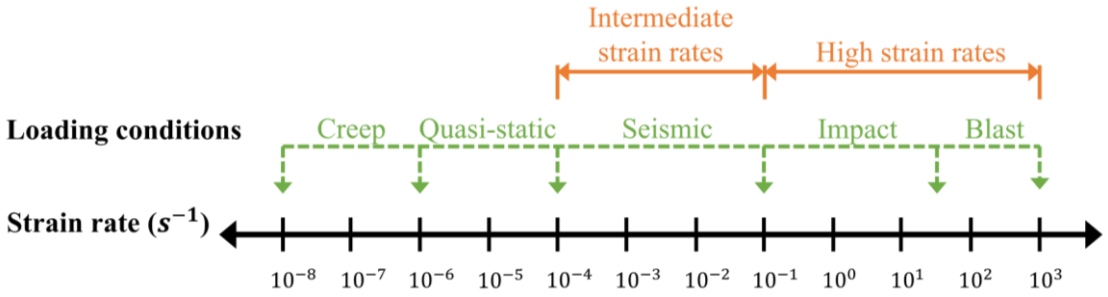

Fig. 18. Typical strain rates and corresponding loading conditions [142].

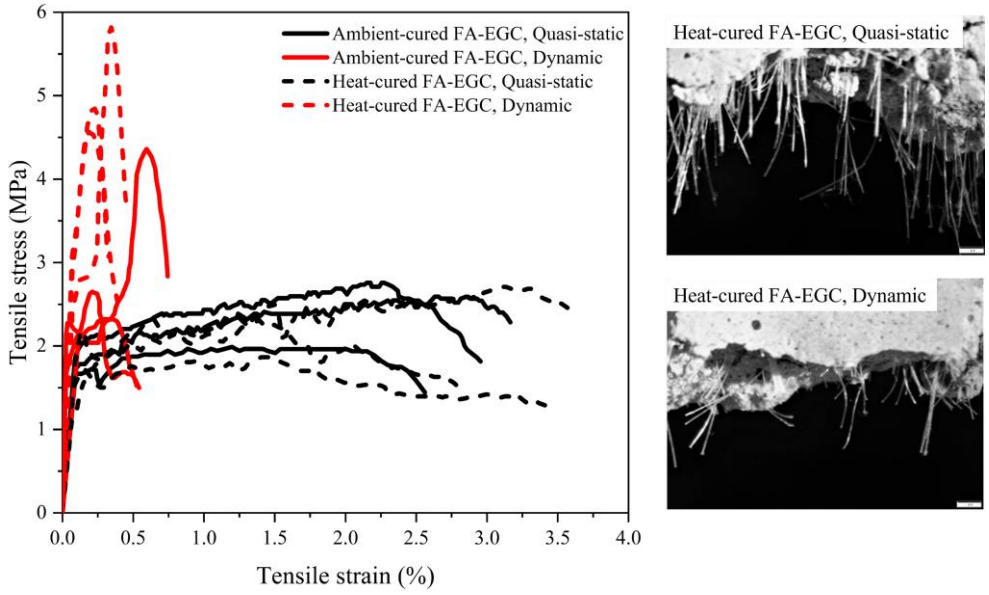

Fig. 19. Effects of curing condition and strain rate on tensile stress-strain response and fibre failure mode at the crack interface [61].

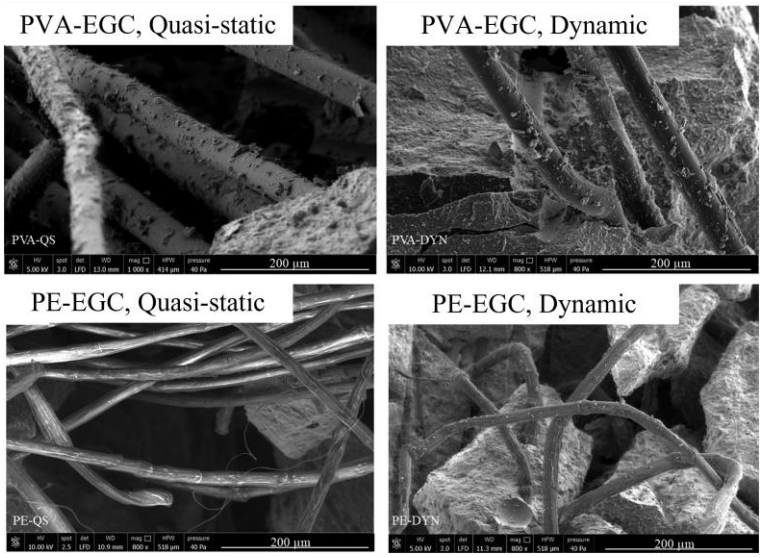

Fig. 20. Fracture surfaces of EGC with PVA and PE fibres under quasi-static and dynamic loadings [14].

Within a range of test strain rates (about 50-160 s^{-1}), all EGC mixtures indicated better dynamic compressive strength than plain geopolymer (see Fig. 21) [53]. The dynamic compressive properties of EGC were improved with the increase of PVA fibre content while replacing PVA fibres with appropriate dosages of RTP fibres (0.25% and 0.5%) in EGC can lead to better dynamic properties as compared with EGC reinforced with 2.0% PVA fibre, which can be ascribed to the synergistic effect between hybrid fibres, enhanced Stefan effect, and smaller fibre spacing of RTP fibres. A schematic illustration of failure mechanism of EGC with hybrid fibres under dynamic compression in Fig. 21 indicates that at a lower strain rate, only some oblique cracks appear inside EGC, and the cracks can propagate along the weak zones. Because of the synergistic effect of PVA and RTP fibres in restraining the cracks, the mixture can maintain its structural integrity. As the strain rate increases, more cracks arise owing to the increased crack velocity and the mixture starts exhibiting fragmental failure. Herein, RTP fibres can effectively restrain the growth of initiated micro-cracks, and PVA fibres can bridge and control the larger cracks. Because of this fibre effect, EGC with hybrid fibres can surpass the mono-PVA fibre reinforced EGC. For future work, a reliable model describing the relationship between dynamic increase factor and strain rate can be developed.

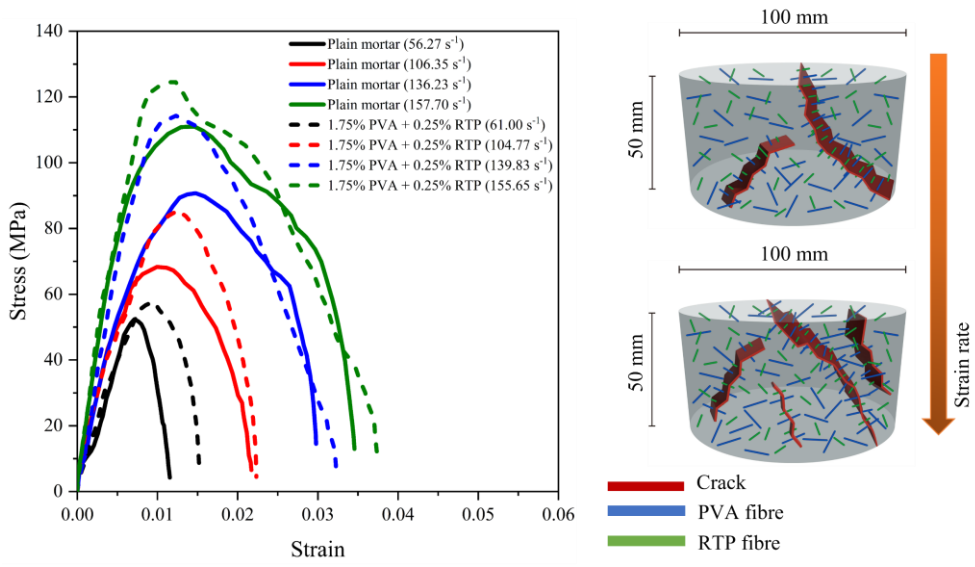

Fig. 21. Effects of fibre and strain rate on dynamic compressive stress-strain response and failure pattern of EGC [53].

4.8. Bond behaviour

The bond between EGC and reinforcement can affect the mechanical behaviour of reinforced concrete structures, which has been rarely studied. Independent of FA/GGBS ratio, all FA-GGBS based EGC outperformed FA-based EGC in terms of bond strength because of the increased contact surface between EGC and steel rebar caused by the reduced porosity [87]. In particular, using 20% GGBS to replace FA in EGC can lead to the highest bond strength (6.2 MPa) among other mixtures. The bond strength was consistently improved with the increasing Agg/b of EGC (0.3-1.0) [98]. Besides, it was reported that the failure between EGC and steel rebar followed a frictional pull-out mode, instead of the splitting failure mode observed between normal concrete and steel rebar. In general, the bond behaviour can be affected by the characteristics of EGC including mechanical properties and microstructure, diameter and embedment length of steel rebar, and thickness of concrete cover [87]. These factors can be considered to develop a reliable model of bond-slip behaviour in further research. Moreover, alternative bar types, e.g., basalt fibre reinforced polymer bars, can be considered for enhancing the long-term durability of concrete structures [143].

4.9. Self-healing behaviour

The use of ECC for concrete structures can enhance the self-healing efficiency owing to the tight crack width and low W/b of ECC [1]. The self-healing efficiency of ECC reduces with the increasing crack width, where it would be difficult for the crack to heal if its width is larger than 150 μm [144]. As discussed in Section 4.5.4, most EGC mixes had an average crack width of lower than 100 μm implying large self-healing potentials.

The self-healing ability of EGC is not only affected by its material composition but also the exposure condition. Water was the common exposure environment for estimating the self-healing of

EGC [81-83], while other exposure conditions (e.g., air and wet-dry cycles) were rarely considered [88]. Fig. 22 displays an example of GGBS-based EGC in terms of its crack width change with the water exposure time, revealing that the crack was fully healed after 36 d of water exposure. Compared to EGC, ECC has relatively superior self-healing behaviour with a 13.5% higher resonant frequency recovery, which can be attributed to the smaller initial crack width of ECC [81]. Using $Ca(OH)_2$ as the activator can induce the best self-healing performance for EGC in comparison with that activated by NaOH or Na_2SiO_3, while the mixture made with Na_2SiO_3 did not present a pronounced self-healing behaviour [83]. The mechanical properties of EGC after the self-healing of cracks can also reflect the self-healing efficiency, which have not been considered in the above studies. Fig. 23 illustrates the effects of exposure environment and preload tensile strain level on the tensile strength and strain capacity of FA-MK based EGC [88], where 0% preload tensile strain means that the EGC specimen was not preloaded but exposed to the same environment. The changing trend of tensile properties with the preload tensile strain level was not clear, while it seems that air exposure can lead to better self-healing behaviour for EGC as opposed to the exposure of wet-dry cycles [88]. In particular, after 7 d of air exposure, the mixture exhibited a tensile strength of 3.3 MPa along with a tensile strain capacity of 6.13%, which surpassed the mixture without preloading.

The continuous reaction of unreacted particles can be regarded as the main mechanism of self-healing in EGC, and the healing products vary with the change in material composition. For the low-calcium (FA-MK based) EGC system, amorphous aluminosilicate phases were the main healing products [88]. By contrast, the healing products in the high-calcium system were similar to those in ECC, e.g., calcium carbonate [81-83]. FA-GGBS based EGC has many benefits over other EGC systems, while its self-healing behaviour has not been comprehensively studied, which would hinder its engineering applications. Therefore, more studies are required to explore the effects of different factors such as FA/GGBS ratio, activator type, and exposure condition and duration. As the self-healing efficiency of EGC is highly associated with the initial crack width, and fibres play a crucial role in determining the crack width after tensile loading, to enhance the self-healing behaviour of EGC, the effects of fibre type, content and properties should be considered.

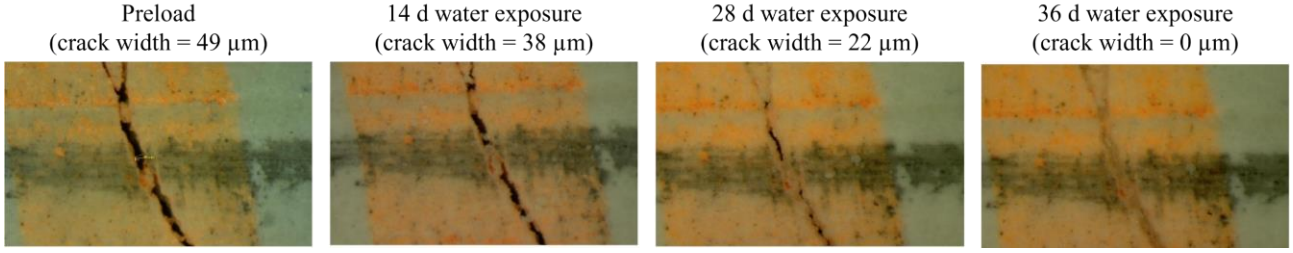

Fig. 22. Variation of crack width of EGC at various water exposure ages [81].

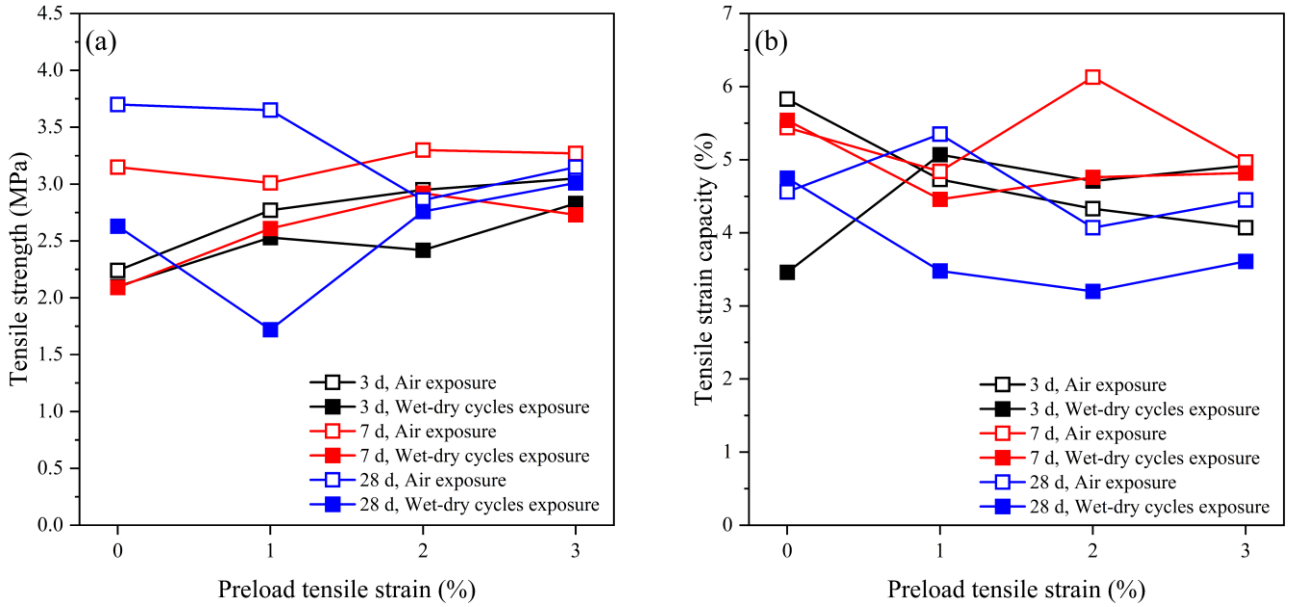

Fig. 23. Tensile properties of EGC under various exposure conditions and preload tensile strain levels [88].

5. Durability

Cementitious materials can experience degradation under various environmental loads (e.g., freeze-thaw cycles) and attacks of aggressive agents (e.g., chloride ions) [110]. Due to the tight crack width of EGC, its permeability can be much lower as opposed to similarly strained concrete, which would be beneficial to the durability of concrete structures made up of EGC [1].

5.1. Fire/thermal resistance

In service, concrete structures would be subjected to fire attack, where the high temperature would not only cause the deterioration of concrete but may also induce the spalling of concrete and thereby expose the reinforcing bar to the fire flame [145]. The commonly used PVA and PE fibres in EGC with low melting points (140-240 ^{o}C) have the potential to improve the resistance to spalling as they can mitigate the inner vapour pressure by leaving empty channels after melting to increase pore connectivity and permeability [146].

A study on the effects of NaOH concentration (6-14 M) and temperature (50 ^{o}C, 100 ^{o}C and 150 ^{o}C) on the impact behaviour of MK-based EGC indicated that the impact force and energy of EGC were improved with the increasing temperature due to the enhanced bonding between fibre and matrix as a result of the formation of more reaction products [13]. By contrast, the impact behaviour of ECC showed an opposite trend. At a lower temperature (50 ^{o}C), ECC outperformed EGC in terms of impact behaviour while as the temperature raised to 100 ^{o}C and 150 ^{o}C, EGC exhibited better performance. The concentration of NaOH should not exceed 12 M at a higher temperature (100 ^{o}C and 150 ^{o}C). The flexural strengths of EGC with PVA and PE fibres were about 6-51% and 20-57% lower as the exposure temperature went up, due to the loss of chemically and physically bonded water and the damage to fibres [92]. Herein, some samples were tested after heating immediately while the rest

were tested after experiencing a cooling period. Regardless of fibre type, the strength loss of EGC after the first regime was greater than that after the second regime, which can be ascribed to the increased fibre elongation and fibre stiffness recovery following the rapid cooling process. When the temperature changed to 200 °C, the mixture with PE fibres yielded a lower residual flexural strength than PVA fibre reinforced EGC, mainly due to the lower melting point of PE fibres (150 °C). As PVA fibres have a higher melting point (240 °C), they do not suffer any obvious degradation at 100 °C and only slight damage at 200 °C.

The compressive strength of FA-GGBS based EGC with 2.0% PVA fibre was improved by 34.3% and 28.5% when the exposure temperature increased from 20 °C to 105 °C and 250 °C, due to the further reaction of unreacted FA particles under a certain high temperature [96], which was also approved in Ref. [99]. However, a further rise of temperature to 400-800 °C significantly weakened the compressive strength of EGC, due to an increase in microcracking and porosity induced by the loss of water and melted PVA fibres as well as the dehydration of reaction products [147]. For GGBS-based EGC, a consistent downward trend in compressive strength can be observed, which can be attributed to the rise in vapour pressure and internal cracking as a result of its dense microstructure [99]. Fig. 24 presents the effect of elevated temperature on the tensile behaviour of EGC, indicating the pronounced tensile strain-hardening and multiple cracking features of EGC under various temperatures, which is consistent with the results of compressive strength [96]. When the temperature was higher (400-800 °C), all EGC did not exhibit strain-hardening behaviour with only one major crack. As seen in Fig. 24b, the tensile strength and tensile strain capacity mostly followed a similar change trend of compressive strength with elevated temperature, which can be explained more clearly using the microscopic images (Fig. 25). At 105 °C, no noticeable damage can be found on PVA fibres while the fibres melted and shrank at 250 °C. At 400 °C, only slight residuals of PVA fibres can be identified, which significantly weakened the fibre bridging effect and thereby reduced the tensile behaviour of EGC especially tensile strain capacity.

The above studies mostly focused on the static mechanical properties of EGC at elevated temperatures, while the dynamic properties are rarely explored. Although using PE fibres could result in higher strength and better ductility for EGC relative to PVA fibres, their lower melting point can pose several concerns to the thermal resistance of EGC. Therefore, the effective measures are required to improve the fire/thermal resistance of PE fibre reinforced EGC.

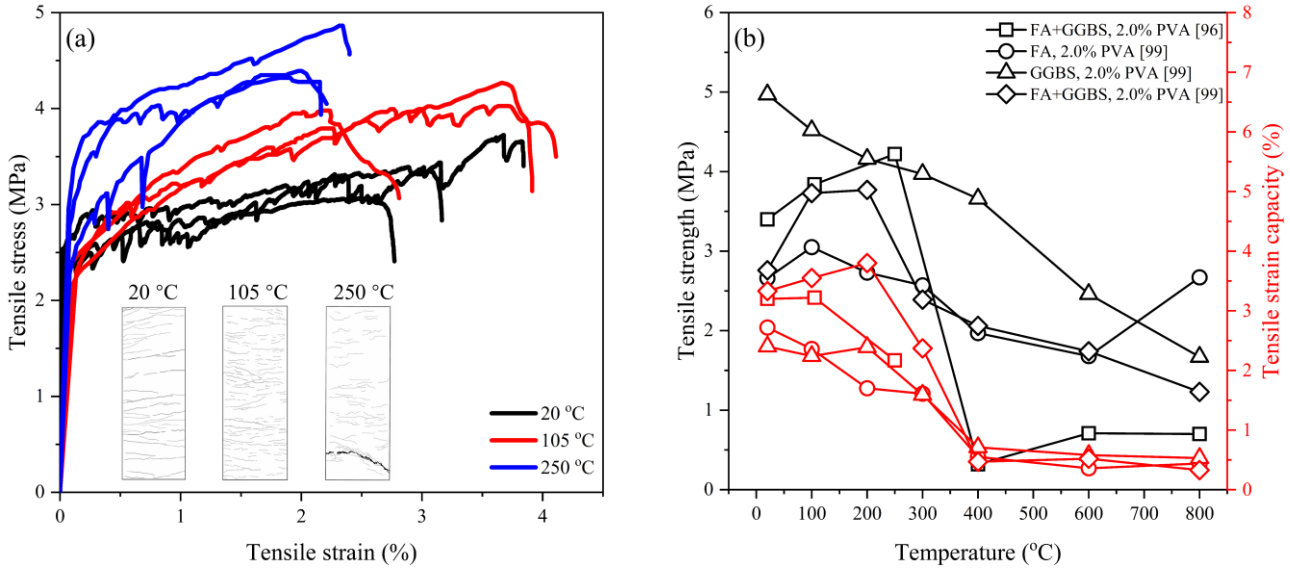

Fig. 24. Effect of elevated temperature on (a) tensile stress-strain response, and (b) tensile strength and tensile strain capacity of EGC [96, 99].

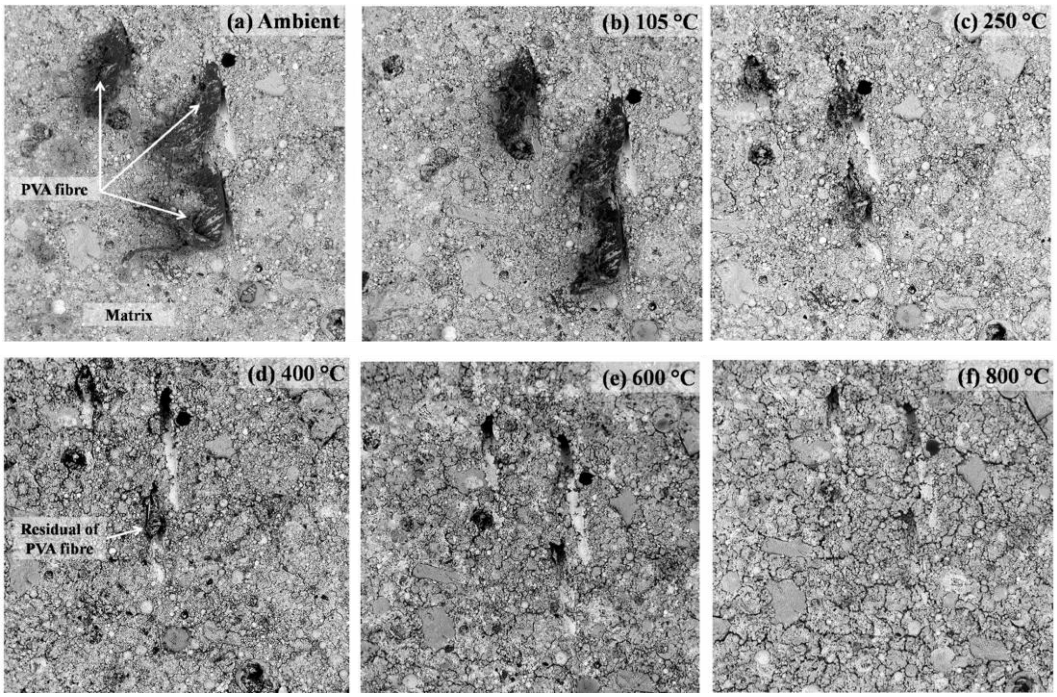

Fig. 25. Microscopic images of PVA fibres in EGC at different temperatures [96].

5.2. Chemical resistance

In recent years, the resistance of EGC to sulphate attack and ingress of chloride ions has been studied. In Ref. [29], POFA-based EGC specimens were exposed to three different sulphate solutions including 5% Na_2SO_4, 5% $MgSO_4$ and a combination of 2.5% Na_2SO_4 and 2.5% $MgSO_4$ for 3-9 months. It was found that regardless of the used NaOH concentration (10, 12 and 14 M) and type of sulphate solution, all mixes experienced a conspicuous loss in compressive strength after different periods of exposure. In particular, the samples after exposure to 5% Na_2SO_4 had the highest strength loss, while the mixtures after exposure to 5% $MgSO_4$ exhibited the least loss in strength. The strength loss of EGC samples was strongly associated with the molarity of NaOH solution due to the loss of a

high amount of reaction products induced by depolymerisation at a higher NaOH concentration. The experimental study on the resistance of GGBS-RHA based EGC with different contents of copper slag to sulphate and seawater attacks indicated that irrespective of copper slag replacement level to silica sand, all specimens had excellent resistance to seawater as compared to sulphate attack, considering the loss in compressive strength [34]. Consistent with mechanical properties, employing 40% copper slag to substitute silica sand resulted in the least strength loss. For instance, after 90 d of exposure to sulphate solution, only 3.8% strength loss was observed for the mixture with 40% copper slag, while 7.7% was found for that containing 60% copper slag due to its looser microstructure. The microstructural investigation indicated no harmful chemical elements in EGC under these aggressive environments. Similar superior resistance was found for the mixture with a 40% replacement level of copper slag under rapid chloride penetration [33]. In summary, the durability of FA- or FA-GGBS based EGC has not been extensively studied, and thus further research is required to account for other types of attack (e.g., carbonation) coupled with different loading conditions.

6. Environmental impact and material cost

This section mainly compares the environmental impact and material cost of ECC and EGC. For sustainability assessment, the functional indicators should be considered, as the comparison is more meaningful when the mixes have similar properties [115]. The tensile strain and strain capacity were used as the functional indicators here given that they are the key properties of ECC and EGC. Two typical ECC mixtures [7, 148] and several EGC mixtures made from FA or FA-GGBS [52, 60, 67] were considered. The embodied carbon, embodied energy and material cost were calculated using the data of each ingredient in Table 3, the results of which are summarised in Table 4.

Due to the higher FA/cement ratio in ECC-2, its embodied carbon and embodied energy were 34.71% and 20.70% respectively lower than those of ECC-1. Although the tensile strength of ECC-2 was slightly lower as compared to ECC-1, it had a higher tensile strain capacity. Regardless of the used binder type, the embodied carbon values of all EGC mixtures were in the range of 294.93-335.16 kg CO_2.eq/m^3, which were 43.27-50.08% and 13.11-23.54% lower than that of ECC-1 and ECC-2, respectively. In addition, they exhibited comparable or even better tensile properties against ECC mixtures. Nevertheless, as seen in Table 4, most EGC had larger embodied energy than ECC mixtures. Fig. 26a and b demonstrate the contribution of each ingredient to the total embodied carbon and embodied energy, indicating that cement and PVA fibres accounted for the largest two proportions of the total embodied carbon and embodied energy for ECC. This explains why the increase of FA/cement ratio in ECC led to lower carbon emission and energy consumption. Regarding EGC, water glass (Na_2SiO_3) contributed the most to the total embodied carbon (about 35-48%), while PVA fibres were the dominant contributor to the total embodied energy (around 36-46%). Replacing PVA

fibres with recycled fibres can help reduce the embodied energy of EGC (EGC-3 against EGC-4), although the tensile properties were weakened.

The estimated material costs of ECC, EGC and commercial grade 45 concrete [149] along with the contribution of each ingredient are presented in Fig. 26c. The actual material costs of these mixes may vary slightly per different manufacturing countries and years. The material cost of ECC-2 was slightly lower than that of ECC-1 due to the lower price of FA as compared to Portland cement. When the PVA fibre volume fraction was 2.0%, the material costs of all considered EGC mixes were around 17-31% higher than that of ECC, which can be attributed to the higher cost of activators especially Na_2SiO_3. Due to the high cost of PVA fibres, there exist a big difference in material cost between ECC (or EGC) and grade 45 concrete. Similar to embodied energy, replacing PVA fibres with recycled fibres can reduce the material cost of EGC.

These results imply the obvious advantage of EGC in reducing carbon footprint. However, the use of common activators (NaOH + Na_2SiO_3) and PVA fibres in EGC would significantly increase the embodied energy and materials cost. To further improve the cost-effectiveness and sustainability of EGC, other types of activators and fibres with lower environmental impacts and costs should be employed, while the strain-hardening and multiple cracking characteristics must be maintained along with acceptable tensile properties in the meantime.

Table 3 Life cycle inventory data and material cost of the ingredients for ECC and EGC.

Material type	Embodied carbon (kg CO_2.eq/kg)	Embodied energy (MJ/kg)	Material cost (USD/kg)
Cement [150, 151]	0.83	4.6	0.072
FA [150, 152]	0.01	0.1	0.0363
GGBS [150, 153]	0.07	1.33	0.0678
Silica sand [151, 154]	0.025	0.17	0.025
SP [151, 154, 155]	1.5	35	1.21
NaOH pellet [67, 152]	0.86	18	1.03
Na_2SiO_3 [152, 156]	0.43	4.6	0.64
PVA fibre [157]	3.4	101	30.92
RTP fibre [150]	2.53	21.9	0.5

Table 4 Calculated embodied carbon, embodied energy and material cost of ECC and EGC.

Ref.	Type (binder)	Fibre (%, by volume)	Embodied carbon (kg CO_2.eq/m^3)	Embodied energy (MJ/m^3)	Material cost (USD/m^3)	Tensile strength (MPa)	Tensile strain capacity (%)
[7]	ECC-1 (cement + FA)	2.0 PVA	590.78	5636.62	889.86	4.86	2.49
[148]	ECC-2 (cement + FA)	2.0 PVA	385.73	4470.02	878.27	4.50	3.00

[67]	EGC-1 (FA)	1.5 PVA	294.93	5101.71	884.96	5.30	4.70
[67]	EGC-2 (FA)	2.0 PVA	316.21	5747.10	1084.70	5.40	4.40
[52]	EGC-3 (FA+GGBS)	2.0 PVA	329.23	6097.04	1143.02	3.40	3.04
[52]	EGC-4 (FA+GGBS)	1.75 PVA + 0.25 RTP	327.52	5849.60	1044.37	2.97	2.24
[60]	EGC-5 (FA+GGBS)	1.5 PVA	313.06	5409.86	955.54	4.37	5.15
[60]	EGC-6 (FA+GGBS)	2.0 PVA	335.16	6066.36	1154.52	4.45	4.91

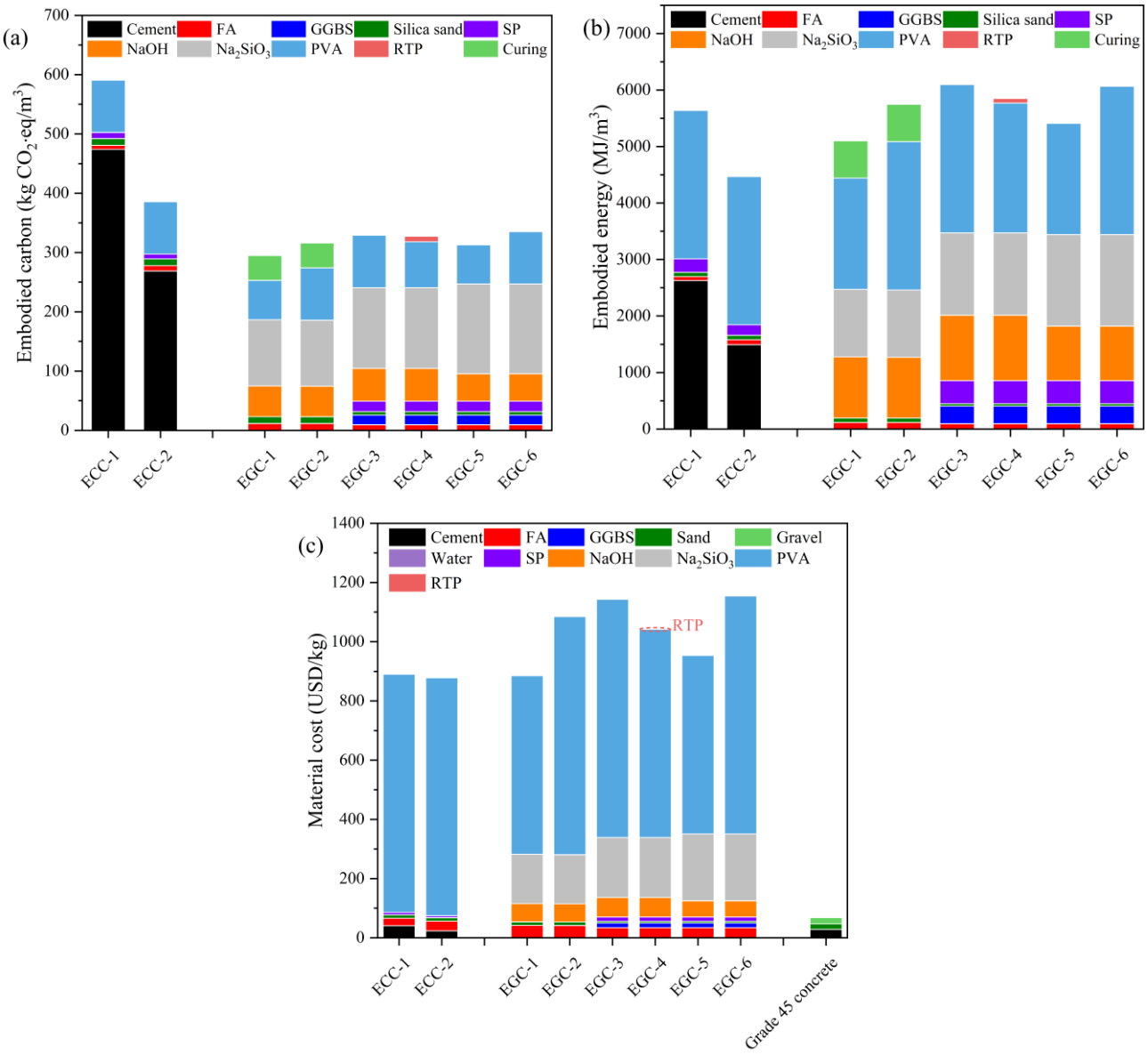

Fig. 26. Environmental impact and material cost of ECC and EGC.

7. 3D printing

The emergence of 3D printing in the construction industry can provide many benefits over traditional mould-casting technology, which can help decrease production time, labour cost and production waste by 30-80% [158]. The general 3D printing procedure for concrete is illustrated in Fig. 27, where

each process can reflect an aspect of printing-related properties including pumpability, extrudability, open time, and buildability [115]. Owing to the layer-by-layer extrusion during 3D printing, implementing the conventional steel reinforcement into 3D printed concrete is challenging [159]. Thus, a new reinforcement concept should be developed for 3D concrete printing and one of the promising strategies is to employ ECC or EGC as the material for 3D printing because of its extraordinary tensile properties and more convenient printing process [6].

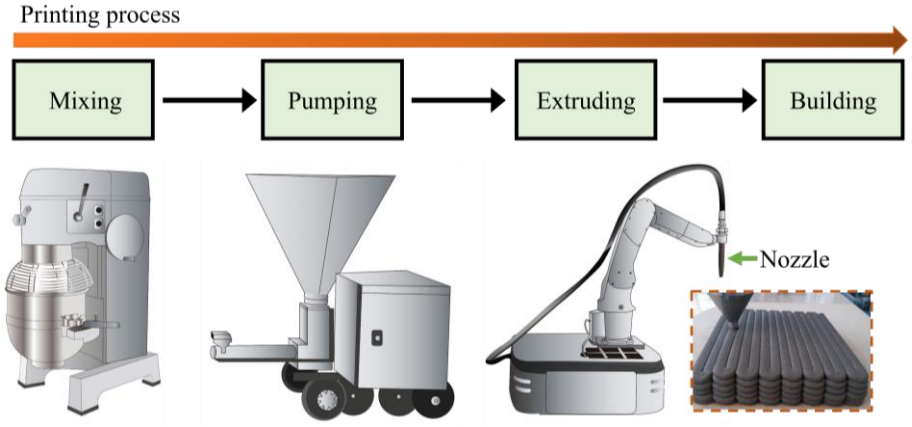

Fig. 27. Typical 3D printing procedure for concrete [6, 115, 160].

To date, only one study has attempted to develop 3D printed EGC with FA, GGBS, anhydrous Na_2SiO_3 and PVA fibres as main ingredients [161]. The effect of printing layer number (one and two) on the density, porosity, compressive strength, and flexural behaviour was estimated, indicating no remarkable difference induced in density and porosity when the printing layer number changed, while the porosity achieved approximately 28% because of the entrapped air caused by the addition of PVA fibres. Regardless of printing layer number, all printed EGC specimens exhibited anisotropic compressive behaviour. The printed specimen made of two layers surpassed that with only one printed layer, in terms of compressive and flexural strengths (see Fig. 28), which can be ascribed to the better compaction of the bottom layer induced by the self-weight of the upper layer. However, the printability of these EGC composites was not evaluated in detail.

Several types of 3D printed ECC have recently been developed and most of them exhibit better tensile properties in comparison with mould-cast ECC (see Fig. 29), which can be mainly attributed to the better fibre dispersion inside the 3D printed ECC. Herein, most fibres tend to distribute along the printing direction that can favour the fibre bridging action, instead of the random fibre distribution found in mould-cast ECC. By contrast, the development of 3D printed EGC is still at a very early stage, which requires more systematic studies to confirm the mix design and printing protocol.

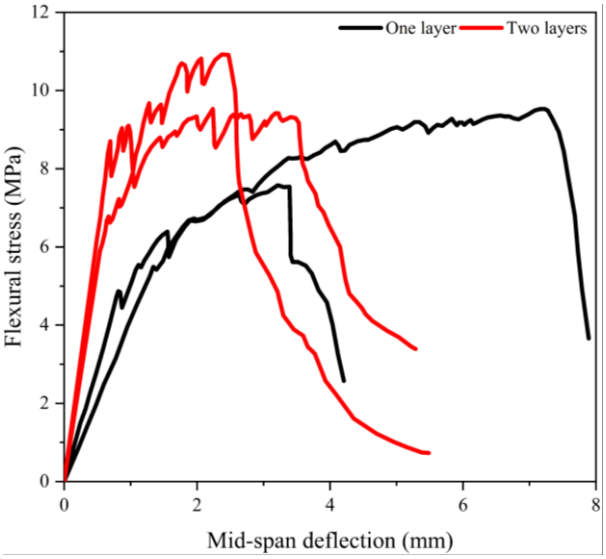

Fig. 28. Effect of printing layer number on flexural stress-deflection curve of 3D printed EGC [161].

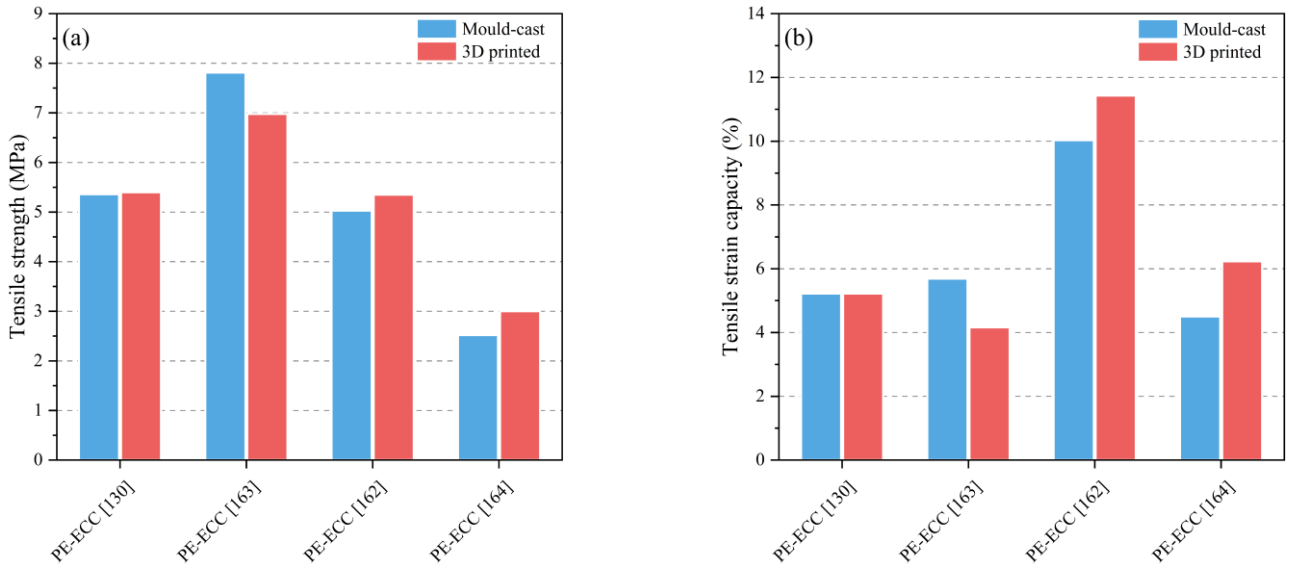

Fig. 29. Tensile properties of 3D printed ECC: (a) tensile strength, and (b) tensile strain capacity [130, 162-164].

8. Conclusions and perspectives

8.1. Conclusions

Driven by the need to improve the greenness of engineered cementitious composites (ECC), there is an increasing number of research on engineered geopolymer composites (EGC) in the past several years. This paper comprehensively reviews the state-of-the-art of EGC, specifically in terms of mix design, manufacturing process, essential material properties and sustainability, and discusses the relations between key mechanical properties and the potential in 3D concrete printing. Some main conclusions can be drawn: (1) Adopting the micromechanical design theory, EGC with tensile strain capacity of up to 13.68% has been developed and its uniaxial tensile behaviour can be tailored by adjusting the material composition (e.g., precursor type, activator nature and fibre content) that would modify its microstructure and in turn change the properties of matrix and fibre-matrix interface. The

tensile properties of most EGC have a positive correlation with the strain-hardening indices, where the index values are higher when a stronger frictional bond and a lower slip-hardening coefficient are present at the interface. In comparison with the widely used ECC (M45), most EGC mixes exhibit a lower matrix fracture toughness and interface properties. (2) The commonly used precursor, activator, aggregate and fibre in EGC are fly ash, a combination of NaOH and Na_2SiO_3, silica sand with size of less than 1180 μm and content of 20-50% (by binder mass), polyvinyl alcohol (PVA) or polyethylene (PE) fibres with volume fraction of no higher than 2.0%, respectively. (3) Employing recycled tyre fibres to partially replace PVA fibres can lead to better drying shrinkage resistance and dynamic properties as compared to mono-PVA fibre reinforced EGC. The inclusion of an appropriate content of defoamer, crumb rubber and copper slag can improve the tensile properties of EGC. (4) The tensile strength of most EGC mixes has positive correlations with compressive strength and tensile strain capacity. The crack spacing and crack width are reduced with the increasing tensile strain capacity. In comparison with M45 ECC, approximately 27% of EGC mixtures exhibit a higher tensile strength ($>$ 4.86 MPa), while about 64% of mixes have a higher tensile strain capacity ($>$ 2.49%). Around 40% of EGC mixes have compressive strength ranging from 40 MPa to 70 MPa, which is adequate for most structural applications. To date, the best overall performance of EGC exhibits a compressive strength, tensile strength and tensile strain capacity of about 100 MPa, 5.77 MPa and 5.81%, respectively. (5) The self-healing of EGC can be triggered by the reaction of unreacted particles and the type of healing products is dependent on the used precursor and activator. The tensile properties of cracked EGC after air exposure are higher than that of mixtures after exposure to wet-dry cycles. (6) EGC with PE fibres exhibits better tensile behaviour than that with PVA fibres under both static and dynamic loadings, while the lower melting point of PE fibre brings concerns to the fire/thermal performance of EGC, especially at a temperature over 200 ^{o}C. (7) The sustainability of EGC is higher than that of ECC, about 13-50% lower in terms of carbon footprint, while the embodied energy and the material cost are greater due to the combined use of Na_2SiO_3 and PVA fibres for EGC.

8.2. Perspectives

Given the potential of EGC in practical applications and the current research gaps, the following aspects can be considered for future research. (1) The quantitative relationships between the matrix's rheology (especially yield stress and viscosity) and uniaxial tensile properties as well as fibre distribution need to be explored. A consistent protocol with specified equipment is required for large-scale engineering applications. (2) The size effects on the compressive strength and uniaxial tensile properties of EGC should be estimated. (3) The uniaxial tensile behaviour of EGC can be related to the microstructural characteristics including pore structure features, fibre orientation coefficient and fibre inclination angle. The microstructure and properties of interfacial transition zone in EGC should be assessed to gain more insights into the overall performance. (4) It is vital to develop optimal mix

proportions of 3D printable EGC along with feasible printing protocol. (5) More studies on the durability of EGC under various mechanical and environmental loadings as well as chemical attacks are needed. (6) Other eco-friendly activators and fibres need to be considered for developing more cost-effective and sustainable EGC.

Acknowledgements

The authors gratefully acknowledge the financial support from the Engineering and Physical Sciences Research Council (EPSRC) under Grant No. EP/R041504/1 and the Royal Society under Award No. IEC\NSFC\191417. The financial support provided by University College London (UCL) and China Scholarship Council (CSC) to the first author is gratefully acknowledged.

References

[1] V.C. Li, Engineered Cementitious Composites (ECC): Bendable Concrete for Sustainable and Resilient Infrastructure, Springer2019.

[2] A.E. Naaman, Tensile strain-hardening FRC composites: Historical evolution since the 1960, Advances in construction materials 2007, Springer2007, pp. 181-202.

[3] M. Şahmaran, V.C. Li, Durability properties of micro-cracked ECC containing high volumes fly ash, Cement and Concrete Research 39(11) (2009) 1033-1043.

[4] M. Maruta, New high-rise RC structure using pre-cast ECC coupling beam, Concrete Journal 43(11) (2005) 18-26.

[5] M. Luković, D. Hordijk, Z. Huang, E. Schlangen, Strain Hardening Cementitious Composite (SHCC) for crack width control in reinforced concrete beams, Heron 64(1/2) (2019) 181.

[6] V.C. Li, F.P. Bos, K. Yu, W. McGee, T.Y. Ng, S.C. Figueiredo, K. Nefs, V. Mechtcherine, V.N. Nerella, J. Pan, G.P.A.G. van Zijl, P.J. Kruger, On the emergence of 3D printable Engineered, Strain Hardening Cementitious Composites (ECC/SHCC), Cement and Concrete Research 132 (2020) 106038.

[7] S. Wang, V.C. Li, Engineered cementitious composites with high-volume fly ash, ACI Mater. J. 104(3) (2007) 233-241.

[8] T. Luukkonen, Z. Abdollahnejad, J. Yliniemi, P. Kinnunen, M. Illikainen, One-part alkali-activated materials: A review, Cement and Concrete Research 103 (2018) 21-34.

[9] K.-H. Yang, J.-K. Song, K.-I. Song, Assessment of CO2 reduction of alkali-activated concrete, Journal of Cleaner Production 39 (2013) 265-272.

[10] J.L. Provis, Alkali-activated materials, Cement and Concrete Research 114 (2017) 40-48.

[11] F.U.A. Shaikh, Deflection hardening behaviour of short fibre reinforced fly ash based geopolymer composites, Materials & Design 50 (2013) 674-682.

[12] B. Nematollahi, J. Sanjayan, J. Qiu, E.-H. Yang, Micromechanics-based investigation of a sustainable ambient temperature cured one-part strain hardening geopolymer composite, Construction and Building Materials 131 (2017) 552-563.
[13] J. Cai, J. Pan, J. Han, Y. Lin, Z. Sheng, Impact behaviours of engineered geopolymer composite exposed to elevated temperatures, Construction and Building Materials 312 (2021) 125421.
[14] A.C.C. Trindade, A.A. Heravi, I. Curosu, M. Liebscher, F. de Andrade Silva, V. Mechtcherine, Tensile behavior of strain-hardening geopolymer composites (SHGC) under impact loading, Cement and Concrete Composites 113 (2020) 103703.
[15] B.-C. Lyu, C. Ding, L.-P. Guo, B. Chen, A.-g. Wang, Basic performances and potential research problems of strain hardening geopolymer composites: A critical review, Construction and Building Materials 287 (2021) 123030.
[16] V.C. Li, Engineered Cementitious Composites (ECC) - material, structural, and durability performance, in: E. Nawy (Ed.), Concrete Construction Engineering Handbook, CRC Press, Boca Raton, 2008.
[17] J.L. Provis, S.A. Bernal, Geopolymers and Related Alkali-Activated Materials, Annual Review of Materials Research 44(1) (2014) 299-327.
[18] L. Weng, K.J.J.o.m.s. Sagoe-Crentsil, Dissolution processes, hydrolysis and condensation reactions during geopolymer synthesis: Part I—Low Si/Al ratio systems, 42(9) (2007) 2997-3006.
[19] N. Ranjbar, C. Kuenzel, J. Spangenberg, M. Mehrali, Hardening evolution of geopolymers from setting to equilibrium: A review, Cement and Concrete Composites 114 (2020) 103729.
[20] J. Provis, J. S. J. van Deventer, Alkali Activated Materials: State-of-the-Art Report, RILEM TC 224-AAM, 2014.
[21] J.L. Provis, G.C. Lukey, J.S. van Deventer, Do geopolymers actually contain nanocrystalline zeolites? A reexamination of existing results, Chem. Mater. 17(12) (2005) 3075-3085.
[22] J.L. Provis, A. Palomo, C. Shi, Advances in understanding alkali-activated materials, Cement and Concrete Research 78 (2015) 110-125.
[23] C.K. Yip, G.C. Lukey, J.S.J. van Deventer, The coexistence of geopolymeric gel and calcium silicate hydrate at the early stage of alkaline activation, Cement and Concrete Research 35(9) (2005) 1688-1697.
[24] S. Zhang, V.C. Li, G. Ye, Micromechanics-guided development of a slag/fly ash-based strain-hardening geopolymer composite, Cement and Concrete Composites 109 (2020) 103510.
[25] P. Duxson, J.L. Provis, G.C. Lukey, J.S.J. van Deventer, The role of inorganic polymer technology in the development of ‘green concrete’, Cement and Concrete Research 37(12) (2007) 1590-1597.

[26] M.I. Khan, R. Siddique, Utilization of silica fume in concrete: Review of durability properties, Resources, Conservation and Recycling 57 (2011) 30-35.
[27] H. Nguyen, V. Carvelli, E. Adesanya, P. Kinnunen, M. Illikainen, High performance cementitious composite from alkali-activated ladle slag reinforced with polypropylene fibers, Cement and Concrete Composites 90 (2018) 150-160.
[28] Y. Zhao, T. Shi, L. Cao, L. Kan, M. Wu, Influence of steel slag on the properties of alkali-activated fly ash and blast-furnace slag based fiber reinforced composites, Cement and Concrete Composites 116 (2021) 103875.
[29] B.A. Salami, M.A. Megat Johari, Z.A. Ahmad, M. Maslehuddin, Durability performance of Palm Oil Fuel Ash-based Engineered Alkaline-activated Cementitious Composite (POFA-EACC) mortar in sulfate environment, Construction and Building Materials 131 (2017) 229-244.
[30] B.A. Salami, M.A. Megat Johari, Z.A. Ahmad, M. Maslehuddin, Impact of added water and superplasticizer on early compressive strength of selected mixtures of palm oil fuel ash-based engineered geopolymer composites, Construction and Building Materials 109 (2016) 198-206.
[31] L. Kan, F. Wang, Mechanical properties of high ductile alkali-activated fiber reinforced composites incorporating red mud under different curing conditions, Ceramics International 48(2) (2022) 1999-2011.
[32] L. Kan, R. Shi, Y. Zhao, X. Duan, M. Wu, Feasibility study on using incineration fly ash from municipal solid waste to develop high ductile alkali-activated composites, Journal of Cleaner Production 254 (2020) 120168.
[33] K.K. Yaswanth, J. Revathy, P. Gajalakshmi, Strength, durability and micro-structural assessment of slag-agro blended based alkali activated engineered geopolymer composites, Case Studies in Construction Materials 16 (2022) e00920.
[34] K.K. Yaswanth, J. Revathy, P. Gajalakshmi, Influence of copper slag on Mechanical, durability and microstructural properties of GGBS and RHA blended strain hardening geopolymer composites, Construction and Building Materials 342 (2022) 128042.
[35] D.-Y. Yoo, S.K. Lee, I. You, T. Oh, Y. Lee, G. Zi, Development of strain-hardening geopolymer mortar based on liquid-crystal display (LCD) glass and blast furnace slag, Construction and Building Materials 331 (2022) 127334.
[36] P. Duxson, J.L. Provis, G.C. Lukey, S.W. Mallicoat, W.M. Kriven, J.S.J. van Deventer, Understanding the relationship between geopolymer composition, microstructure and mechanical properties, Colloids and Surfaces A: Physicochemical and Engineering Aspects 269(1-3) (2005) 47-58.

[37] J. Zhao, L. Tong, B. Li, T. Chen, C. Wang, G. Yang, Y. Zheng, Eco-friendly geopolymer materials: A review of performance improvement, potential application and sustainability assessment, Journal of Cleaner Production 307 (2021) 127085.
[38] P. Sturm, S. Greiser, G. Gluth, C. Jäger, H. Brouwers, Degree of reaction and phase content of silica-based one-part geopolymers investigated using chemical and NMR spectroscopic methods, Journal of Materials Science 50(20) (2015) 6768-6778.
[39] M.I. Khan, G. Fares, S. Mourad, W.J.J.o.M.i.C.E. Abbass, Optimized Fresh and Hardened Properties of Strain-Hardening Cementitious Composites: Effect of Sand Size and Workability, Journal of Materials in Civil Engineering 28(12) (2016) 04016152.
[40] J. Thomas, B. Harilal, Sustainability evaluation of cold-bonded aggregates made from waste materials, Journal of Cleaner Production 237 (2019) 117788.
[41] B.S. Thomas, R.C. Gupta, A comprehensive review on the applications of waste tire rubber in cement concrete, Renewable and Sustainable Energy Reviews 54 (2016) 1323-1333.
[42] B. Nematollahi, R. Ranade, J. Sanjayan, S. Ramakrishnan, Thermal and mechanical properties of sustainable lightweight strain hardening geopolymer composites, Archives of Civil and Mechanical Engineering 17(1) (2017) 55-64.
[43] Q.-H. Lương, H.H. Nguyễn, J.-I. Choi, H.-K. Kim, B.Y. Lee, Effects of crumb rubber particles on mechanical properties and sustainability of ultra-high-ductile slag-based composites, Construction and Building Materials 272 (2021) 121959.
[44] W. Wang, A. Shen, Z. Lyu, Z. He, K.T.Q. Nguyen, Fresh and rheological characteristics of fiber reinforced concrete——A review, Construction and Building Materials 296 (2021) 123734.
[45] Y. Lee, J.-I. Choi, H.-K. Kim, B.Y. Lee, Effects of a defoamer on the compressive strength and tensile behavior of alkali-activated slag-based cementless composite reinforced by polyethylene fiber, Composite Structures 172 (2017) 166-172.
[46] D. Shoji, Z. He, D. Zhang, V.C. Li, The greening of engineered cementitious composites (ECC): A review, Construction and Building Materials 327 (2022) 126701.
[47] C. Redon, V.C. Li, C. Wu, H. Hoshiro, T. Saito, A. Ogawa, Measuring and modifying interface properties of PVA fibers in ECC matrix, Journal of Materials in Civil Engineering 13(6) (2001) 399-406.
[48] Z. Qi, W. Chen, L. Zhang, Z. Huang, An integrated design method for functional cementitious composites (FCC), Construction and Building Materials 249 (2020) 118698.
[49] R. Merli, M. Preziosi, A. Acampora, M.C. Lucchetti, E. Petrucci, Recycled fibers in reinforced concrete: A systematic literature review, Journal of Cleaner Production 248 (2019) 119207.

[50] D. Zhang, J. Yu, H. Wu, B. Jaworska, B.R. Ellis, V.C. Li, Discontinuous micro-fibers as intrinsic reinforcement for ductile Engineered Cementitious Composites (ECC), Composites Part B: Engineering 184 (2020) 107741.
[51] Y. Wang, C.L. Chan, S.H. Leong, M. Zhang, Engineering properties of strain hardening geopolymer composites with hybrid polyvinyl alcohol and recycled steel fibres, Construction and Building Materials 261 (2020) 120585.
[52] H. Zhong, M. Zhang, Effect of recycled tyre polymer fibre on engineering properties of sustainable strain hardening geopolymer composites, Cement and Concrete Composites 122 (2021) 104167.
[53] H. Zhong, M. Zhang, Effect of recycled polymer fibre on dynamic compressive behaviour of engineered geopolymer composites, Ceramics International 48(16) (2022) 1151-1168.
[54] F. Li, Z. Yang, A. Zheng, S. Li, Properties of modified engineered geopolymer composites incorporating multi-walled carbon Nanotubes(MWCNTs) and granulated blast furnace Slag(GBFS), Ceramics International 47(10) (2021) 14244-14259.
[55] Z. Luo, W. Li, P. Li, K. Wang, S.P. Shah, Investigation on effect of nanosilica dispersion on the properties and microstructures of fly ash-based geopolymer composite, Construction and Building Materials 282 (2021) 122690.
[56] H. Ye, A. Radlińska, Shrinkage mechanisms of alkali-activated slag, Cement and Concrete Research 88 (2016) 126-135.
[57] F. Puertas, S. Martínez-Ramírez, S. Alonso, T. Vázquez, Alkali-activated fly ash/slag cements: Strength behaviour and hydration products, Cement and Concrete Research 30(10) (2000) 1625-1632.
[58] G. Fang, M. Zhang, Multiscale micromechanical analysis of alkali-activated fly ash-slag paste, Cement and Concrete Research 135 (2020) 106141.
[59] Z. Tang, W. Li, Chapter 21 - Utilization of recycled aggregate in geopolymer concrete development: A case study, in: D.C.W. Tsang, L. Wang (Eds.), Low Carbon Stabilization and Solidification of Hazardous Wastes, Elsevier2022, pp. 343-354.
[60] Y. Wang, H. Zhong, M. Zhang, Experimental study on static and dynamic properties of fly ash-slag based strain hardening geopolymer composites, Cement and Concrete Composites 129 (2022) 104481.
[61] M. Farooq, A. Krishna, N. Banthia, Highly ductile fiber reinforced geopolymers under tensile impact, Cement and Concrete Composites 126 (2022) 104374.
[62] B. Nematollahi, J. Sanjayan, J. Qiu, E.-H. Yang, High ductile behavior of a polyethylene fiber-reinforced one-part geopolymer composite: A micromechanics-based investigation, Archives of Civil and Mechanical Engineering 17(3) (2017) 555-563.

[63] L.-Y. Xu, B.-T. Huang, V.C. Li, J.-G. Dai, High-strength high-ductility Engineered/Strain-Hardening Cementitious Composites (ECC/SHCC) incorporating geopolymer fine aggregates, Cement and Concrete Composites 125 (2022) 104296.
[64] V.C. Li, S. Wang, Microstructure variability and macroscopic composite properties of high performance fiber reinforced cementitious composites, Probabilistic Engineering Mechanics 21(3) (2006) 201-206.
[65] B.Y. Lee, C.-G. Cho, H.-J. Lim, J.-K. Song, K.-H. Yang, V.C. Li, Strain hardening fiber reinforced alkali-activated mortar – A feasibility study, Construction and Building Materials 37 (2012) 15-20.
[66] M. Ohno, V.C. Li, A feasibility study of strain hardening fiber reinforced fly ash-based geopolymer composites, Construction and Building Materials 57 (2014) 163-168.
[67] M. Ohno, V.C. Li, An integrated design method of Engineered Geopolymer Composite, Cement and Concrete Composites 88 (2018) 73-85.
[68] C.-G. Cho, H.-J. Lim, B.-Y. Lee, Y. Choi, Experiments and performances of strain-hardening fiber low cementitious composites, Advances in Mechanical Engineering 7(6) (2015) 168781401558542.
[69] S.-J. Choi, J.-I. Choi, J.-K. Song, B.Y. Lee, Rheological and mechanical properties of fiber-reinforced alkali-activated composite, Construction and Building Materials 96 (2015) 112-118.
[70] J.I. Choi, S.E. Park, H.H. Nguyen, S.L. Cha, B.Y. Lee, Strain-Hardening and High-Ductile Behavior of Alkali-Activated Slag-Based Composites with Added Zirconia Silica Fume, Materials (Basel) 12(21) (2019).
[71] J.-I. Choi, S.-E. Park, S.-T. Kang, B.Y. Lee, Effects of Aging on the Tensile Properties of Polyethylene Fiber-Reinforced Alkali-Activated Slag-Based Composite, Advances in Materials Science and Engineering 2019 (2019) 7573635.
[72] J.-I. Choi, H.-K. Kim, B.Y. Lee, Mechanical and Fiber-Bridging Behavior of Slag-Based Composite with High Tensile Ductility, Applied Sciences 10(12) (2020) 4300.
[73] J.-I. Choi, H.H. Nguyễn, S.L. Cha, M. Li, B.Y. Lee, Composite properties of calcium-based alkali-activated slag composites reinforced by different types of polyethylene fibers and micromechanical analysis, Construction and Building Materials 273 (2021) 121760.
[74] B. Nematollahi, J. Sanjayan, F.U.A. Shaikh, Matrix design of strain hardening fiber reinforced engineered geopolymer composite, Composites Part B: Engineering 89 (2016) 253-265.
[75] B. Nematollahi, J. Qiu, E.-H. Yang, J. Sanjayan, Micromechanics constitutive modelling and optimization of strain hardening geopolymer composite, Ceramics International 43(8) (2017) 5999-6007.

[76] B. Nematollahi, J. Qiu, E.-H. Yang, J. Sanjayan, Microscale investigation of fiber-matrix interface properties of strain-hardening geopolymer composite, Ceramics International 43(17) (2017) 15616-15625.
[77] B. Nematollahi, J. Sanjayan, F.U.A. Shaikh, Comparative deflection hardening behavior of short fiber reinforced geopolymer composites, Construction and Building Materials 70 (2014) 54-64.
[78] B. Nematollahi, J. Sanjayan, F.U.A. Shaikh, Tensile Strain Hardening Behavior of PVA Fiber-Reinforced Engineered Geopolymer Composite, Journal of Materials in Civil Engineering 27(10) (2015) 1-12.
[79] M.H. Al-Majidi, A. Lampropoulos, A.B. Cundy, Tensile properties of a novel fibre reinforced geopolymer composite with enhanced strain hardening characteristics, Composite Structures 168 (2017) 402-427.
[80] Y. Alrefaei, J.-G. Dai, Tensile behavior and microstructure of hybrid fiber ambient cured one-part engineered geopolymer composites, Construction and Building Materials 184 (2018) 419-431.
[81] H.H. Nguyễn, J.-I. Choi, K.-I. Song, J.-K. Song, J. Huh, B.Y. Lee, Self-healing properties of cement-based and alkali-activated slag-based fiber-reinforced composites, Construction and Building Materials 165 (2018) 801-811.
[82] H.H. Nguyễn, J.-I. Choi, H.-K. Kim, B.Y. Lee, Effects of the type of activator on the self-healing ability of fiber-reinforced alkali-activated slag-based composites at an early age, Construction and Building Materials 224 (2019) 980-994.
[83] H.H. Nguyễn, J.-I. Choi, H.-K. Kim, B.Y. Lee, Mechanical properties and self-healing capacity of eco-friendly ultra-high ductile fiber-reinforced slag-based composites, Composite Structures 229 (2019) 111401.
[84] M. Zahid, N. Shafiq, M.H. Isa, L. Gil, Statistical modeling and mix design optimization of fly ash based engineered geopolymer composite using response surface methodology, Journal of Cleaner Production 194 (2018) 483-498.
[85] M. Zahid, N. Shafiq, S.N.A. Razak, R.F. Tufail, Investigating the effects of NaOH molarity and the geometry of PVA fibers on the post-cracking and the fracture behavior of engineered geopolymer composite, Construction and Building Materials 265 (2020) 120295.
[86] M. Farooq, A. Bhutta, N. Banthia, Tensile performance of eco-friendly ductile geopolymer composites (EDGC) incorporating different micro-fibers, Cement and Concrete Composites 103 (2019) 183-192.
[87] Y. Ling, K. Wang, W. Li, G. Shi, P. Lu, Effect of slag on the mechanical properties and bond strength of fly ash-based engineered geopolymer composites, Composites Part B: Engineering 164 (2019) 747-757.

[88] L.-l. Kan, J.-w. Lv, B.-b. Duan, M. Wu, Self-healing of Engineered Geopolymer Composites prepared by fly ash and metakaolin, Cement and Concrete Research 125 (2019) 105895.
[89] L.-l. Kan, W.-s. Wang, W.-d. Liu, M. Wu, Development and characterization of fly ash based PVA fiber reinforced Engineered Geopolymer Composites incorporating metakaolin, Cement and Concrete Composites 108 (2020) 103521.
[90] L. Kan, L. Zhang, Y. Zhao, M. Wu, Properties of polyvinyl alcohol fiber reinforced fly ash based Engineered Geopolymer Composites with zeolite replacement, Construction and Building Materials 231 (2020) 117161.
[91] Y. Wang, Y. Wang, M. Zhang, Effect of sand content on engineering properties of fly ash-slag based strain hardening geopolymer composites, Journal of Building Engineering 34 (2021) 101951.
[92] A.C. Constâncio Trindade, M. Liebscher, I. Curosu, F. de Andrade Silva, V. Mechtcherine, Influence of elevated temperatures on the residual and quasi in-situ flexural strength of strain-hardening geopolymer composites (SHGC) reinforced with PVA and PE fibers, Construction and Building Materials 314 (2022) 125649.
[93] L. Kan, F. Wang, Z. Zhang, W. Kabala, Y. Zhao, Mechanical properties of high ductile alkali-activated fiber reinforced composites with different curing ages, Construction and Building Materials 306 (2021) 124833.
[94] H.H. Nguyễn, Q.-H. Lương, J.-I. Choi, R. Ranade, V.C. Li, B.Y. Lee, Ultra-ductile behavior of fly ash-based engineered geopolymer composites with a tensile strain capacity up to 13.7%, Cement and Concrete Composites 122 (2021) 104133.
[95] J. Cai, J. Pan, J. Han, Y. Lin, Z. Sheng, Low-energy impact behavior of ambient cured engineered geopolymer composites, Ceramics International 48(7) (2022) 9378-9389.
[96] C.L. Chan, M. Zhang, Behaviour of strain hardening geopolymer composites at elevated temperatures, Cement and Concrete Composites 132 (2022) 104634.
[97] J.-C. Lao, L.-Y. Xu, B.-T. Huang, J.-G. Dai, S.P. Shah, Strain-hardening Ultra-High-Performance Geopolymer Concrete (UHPGC): Matrix design and effect of steel fibers, Composites Communications 30 (2022) 101081.
[98] S. Kumar, C. Sekhar Das, J. Lao, Y. Alrefaei, J.-G. Dai, Effect of sand content on bond performance of engineered geopolymer composites (EGC) repair material, Construction and Building Materials 328 (2022) 127080.
[99] G. Humur, A. Çevik, Mechanical characterization of lightweight engineered geopolymer composites exposed to elevated temperatures, Ceramics International 48(10) (2022) 13634-13650.
[100] G. Humur, A. Çevik, Effects of hybrid fibers and nanosilica on mechanical and durability properties of lightweight engineered geopolymer composites subjected to cyclic loading and heating–cooling cycles, Construction and Building Materials 326 (2022) 126846.

[101] E. Yang, V.C. Li, Numerical study on steady-state cracking of composites, Composites Science and Technology 67(2) (2007) 151-156.
[102] E.B. Pereira, G. Fischer, J.A.O. Barros, Direct assessment of tensile stress-crack opening behavior of Strain Hardening Cementitious Composites (SHCC), Cement and Concrete Research 42(6) (2012) 834-846.
[103] E.-H. Yang, S. Wang, Y. Yang, V.C. Li, Fiber-bridging constitutive law of engineered cementitious composites, Journal of advanced concrete technology 6(1) (2008) 181-193.
[104] V.C. Li, S. Wang, C. Wu, Tensile strain-hardening behavior of polyvinyl alcohol engineered cementitious composite (PVA-ECC), ACI Mater. J. 98(6) (2001) 483-492.
[105] Z. Pan, J.G. Sanjayan, B.V. Rangan, Fracture properties of geopolymer paste and concrete, 63(10) (2011) 763-771.
[106] D.A. Lange, H.M. Jennings, S.P. Shah, Relationship between Fracture Surface Roughness and Fracture Behavior of Cement Paste and Mortar, Journal of the American Ceramic Society 76(3) (1993) 589-597.
[107] J.-I. Choi, K.-I. Song, J.-K. Song, B.Y. Lee, Composite properties of high-strength polyethylene fiber-reinforced cement and cementless composites, Composite Structures 138 (2016) 116-121.
[108] T. Kanda, V.C. Li, Practical design criteria for saturated pseudo strain hardening behavior in ECC, Journal of advanced concrete technology 4(1) (2006) 59-72.
[109] T. Kanda, V.C. Li, Multiple cracking sequence and saturation in fiber reinforced cementitious composites, Concrete Research and Technology 9 (1998) 19-33.
[110] N. Ranjbar, M. Zhang, Fiber-reinforced geopolymer composites: A review, Cement and Concrete Composites 107 (2020) 103498.
[111] K.H. Khayat, W. Meng, K. Vallurupalli, L. Teng, Rheological properties of ultra-high-performance concrete — An overview, Cement and Concrete Research 124 (2019) 105828.
[112] M. Yamanoi, J.M. Maia, Analysis of rheological properties of fibre suspensions in a Newtonian fluid by direct fibre simulation. Part1: Rigid fibre suspensions, Journal of Non-Newtonian Fluid Mechanics 165(19) (2010) 1055-1063.
[113] C. Lu, Z. Zhang, C. Shi, N. Li, D. Jiao, Q. Yuan, Rheology of alkali-activated materials: A review, Cement and Concrete Composites 121 (2021) 104061.
[114] K. Kondepudi, K.V.L. Subramaniam, B. Nematollahi, S.H. Bong, J. Sanjayan, Study of particle packing and paste rheology in alkali activated mixtures to meet the rheology demands of 3D Concrete Printing, Cement and Concrete Composites 131 (2022) 104581.
[115] H. Zhong, M. Zhang, 3D printing geopolymers: A review, Cement and Concrete Composites 128 (2022) 104455.

[116] J. Zhang, C. Gong, Z. Guo, M. Zhang, Engineered cementitious composite with characteristic of low drying shrinkage, Cement and Concrete Research 39(4) (2009) 303-312.
[117] H. Zhu, D. Zhang, Y. Wang, T. Wang, V.C. Li, Development of self-stressing Engineered Cementitious Composites (ECC), Cement and Concrete Composites 118 (2021) 103936.
[118] P.-m. Zhan, Z.-h. He, Application of shrinkage reducing admixture in concrete: A review, Construction and Building Materials 201 (2019) 676-690.
[119] W.-J. Long, H.-D. Li, L. Mei, W. Li, F. Xing, K.H. Khayat, Damping characteristics of PVA fiber-reinforced cementitious composite containing high-volume fly ash under frequency-temperature coupling effects, Cement and Concrete Composites 118 (2021) 103911.
[120] F. Liu, K. Xu, W. Ding, Y. Qiao, L. Wang, Microstructural characteristics and their impact on mechanical properties of steel-PVA fiber reinforced concrete, Cement and Concrete Composites 123 (2021) 104196.
[121] ASTM C109/C109M-20b, Standard Test Method for Compressive Strength of Hydraulic Cement Mortars (Using 2-in . or [50-mm] Cube Specimens), ASTM International, West Conshohocken, PA, 2020.
[122] ACI 318, Building Code Requirements for Structural Concrete and Commentary American Concrete Institute, 2008.
[123] CEB-FIP model code 1990: Design code, Comite Euro-Inernational Du Beton 1990.
[124] N.K. Lee, H.K. Lee, Setting and mechanical properties of alkali-activated fly ash/slag concrete manufactured at room temperature, Construction and Building Materials 47 (2013) 1201-1209.
[125] N. Fonseca, J. de Brito, L. Evangelista, The influence of curing conditions on the mechanical performance of concrete made with recycled concrete waste, Cement and Concrete Composites 33(6) (2011) 637-643.
[126] K. Wille, S. El-Tawil, A.E. Naaman, Properties of strain hardening ultra high performance fiber reinforced concrete (UHP-FRC) under direct tensile loading, Cement and Concrete Composites 48 (2014) 53-66.
[127] C. Lu, V.C. Li, C.K.Y. Leung, Flaw characterization and correlation with cracking strength in Engineered Cementitious Composites (ECC), Cement and Concrete Research 107 (2018) 64-74.
[128] V.C. Li, C.K. Leung, Steady-state and multiple cracking of short random fiber composites, J. Eng. Mech. 118(11) (1992) 2246-2264.
[129] J. Yu, J. Yao, X. Lin, H. Li, J.Y.K. Lam, C.K.Y. Leung, I.M.L. Sham, K. Shih, Tensile performance of sustainable Strain-Hardening Cementitious Composites with hybrid PVA and recycled PET fibers, Cement and Concrete Research 107 (2018) 110-123.

[130] B. Zhu, J. Pan, J. Li, P. Wang, M. Zhang, Relationship between microstructure and strain-hardening behaviour of 3D printed engineered cementitious composites, Cement and Concrete Composites 133 (2022) 104677.
[131] J. Li, J. Weng, Z. Chen, E.-H. Yang, A generic model to determine crack spacing of short and randomly oriented polymeric fiber-reinforced strain-hardening cementitious composites (SHCC), Cement and Concrete Composites 118 (2021) 103919.
[132] Z. Luo, W. Li, K. Wang, S.P. Shah, D. Sheng, Nano/micromechanical characterisation and image analysis on the properties and heterogeneity of ITZs in geopolymer concrete, Cement and Concrete Research 152 (2022) 106677.
[133] W. Li, Z. Luo, Y. Gan, K. Wang, S.P. Shah, Nanoscratch on mechanical properties of interfacial transition zones (ITZs) in fly ash-based geopolymer composites, Composites Science and Technology 214 (2021) 109001.
[134] G. Fang, M. Zhang, The evolution of interfacial transition zone in alkali-activated fly ash-slag concrete, Cement and Concrete Research 129 (2020) 105963.
[135] D.-Y. Yoo, N. Banthia, High-performance strain-hardening cementitious composites with tensile strain capacity exceeding 4%: A review, Cement and Concrete Composites 125 (2022) 104325.
[136] K. Yu, Y. Ding, J. Liu, Y. Bai, Energy dissipation characteristics of all-grade polyethylene fiber-reinforced engineered cementitious composites (PE-ECC), Cement and Concrete Composites 106 (2020) 103459.
[137] J. Qiu, H.S. Tan, E.-H. Yang, Coupled effects of crack width, slag content, and conditioning alkalinity on autogenous healing of engineered cementitious composites, Cement and Concrete Composites 73 (2016) 203-212.
[138] D.-Y. Yoo, N. Banthia, Impact resistance of fiber-reinforced concrete – A review, Cement and Concrete Composites 104 (2019) 103389.
[139] Y. Hao, H. Hao, G.P. Jiang, Y. Zhou, Experimental confirmation of some factors influencing dynamic concrete compressive strengths in high-speed impact tests, Cement and Concrete Research 52 (2013) 63-70.
[140] W. Ren, J. Xu, J. Liu, H. Su, Dynamic mechanical properties of geopolymer concrete after water immersion, Ceramics International 41(9, Part B) (2015) 11852-11860.
[141] Q. Li, X. Jiang, T. Zeng, S. Xu, Experimental investigation on strain rate effect of high-performance fiber reinforced cementitious composites subject to dynamic direct tensile loading, Cement and Concrete Research 157 (2022) 106825.
[142] D.-J. Kim, A.E. Naaman, S. El-Tawil, High performance fiber reinforced cement composites with innovative slip hardending twisted steel fibers, International Journal of Concrete Structures and Materials 3(2) (2009) 119-126.

[143] A. Serbescu, M. Guadagnini, K. Pilakoutas, Mechanical characterization of basalt FRP rebars and long-term strength predictive model, Journal of Composites for Construction 19(2) (2015) 04014037.
[144] Y. Yang, M.D. Lepech, E.-H. Yang, V.C. Li, Autogenous healing of engineered cementitious composites under wet–dry cycles, Cement and Concrete Research 39(5) (2009) 382-390.
[145] Q. Ma, R. Guo, Z. Zhao, Z. Lin, K. He, Mechanical properties of concrete at high temperature—A review, Construction and Building Materials 93 (2015) 371-383.
[146] H. Wu, X. Lin, A. Zhou, A review of mechanical properties of fibre reinforced concrete at elevated temperatures, Cement and Concrete Research 135 (2020) 106117.
[147] S.M. Park, J.G. Jang, N.K. Lee, H.K. Lee, Physicochemical properties of binder gel in alkali-activated fly ash/slag exposed to high temperatures, Cement and Concrete Research 89 (2016) 72-79.
[148] E.-H. Yang, Y. Yang, V.C. Li, Use of high volumes of fly ash to improve ECC mechanical properties and material greenness, ACI Mater. J. 104(6) (2007) 620-628.
[149] J. Yu, D.K. Mishra, C. Hu, C.K.Y. Leung, S.P. Shah, Mechanical, environmental and economic performance of sustainable Grade 45 concrete with ultrahigh-volume Limestone-Calcined Clay (LCC), Resources, Conservation and Recycling 175 (2021) 105846.
[150] G. Hammond, C. Jones, F. Lowrie, P. Tse, Inventory of carbon & energy: ICE, Sustainable Energy Research Team, Department of Mechanical Engineering 2008.
[151] D. Zhang, B. Jaworska, H. Zhu, K. Dahlquist, V.C. Li, Engineered Cementitious Composites (ECC) with limestone calcined clay cement (LC3), Cement and Concrete Composites 114 (2020) 103766.
[152] Z. Abdollahnejad, F. Pacheco-Torgal, T. Félix, W. Tahri, J. Barroso Aguiar, Mix design, properties and cost analysis of fly ash-based geopolymer foam, Construction and Building Materials 80 (2015) 18-30.
[153] A. Rafeet, R. Vinai, M. Soutsos, W. Sha, Guidelines for mix proportioning of fly ash/GGBS based alkali activated concretes, Construction and Building Materials 147 (2017) 130-142.
[154] R. Ranade, Advanced cementitious composite development for resilient and sustainable infrastructure, University of Michigan, 2014.
[155] G.A. Keoleian, A. Kendall, J.E. Dettling, V.M. Smith, R.F. Chandler, M.D. Lepech, V.C. Li, Life cycle modeling of concrete bridge design: Comparison of engineered cementitious composite link slabs and conventional steel expansion joints, J. Infrastruct. Syst. 11 (2005) 51-60.
[156] M. Fawer, M. Concannon, W. Rieber, Life cycle inventories for the production of sodium silicates, The International Journal of Life Cycle Assessment 4(4) (1999) 207.
[157] R. Frazão, R. Fernandes, Comparative Analysis of the Life Cycle of AT Fibre-cement and NT Fibre-cement, International Chrysotile Association (2004).

[158] J. Zhang, J. Wang, S. Dong, X. Yu, B. Han, A review of the current progress and application of 3D printed concrete, Composites Part A: Applied Science and Manufacturing 125 (2019) 105533.
[159] Z. Li, L. Wang, G. Ma, Mechanical improvement of continuous steel microcable reinforced geopolymer composites for 3D printing subjected to different loading conditions, Composites Part B: Engineering 187 (2020) 107796.
[160] G. Ma, Z. Li, L. Wang, F. Wang, J. Sanjayan, Mechanical anisotropy of aligned fiber reinforced composite for extrusion-based 3D printing, Construction and Building Materials 202 (2019) 770-783.
[161] S.H. Bong, B. Nematollahi, M. Xia, A. Nazari, J. Sanjayan, J. Pan, Properties of 3D-Printable Ductile Fibre-Reinforced Geopolymer Composite for Digital Construction Applications, in: V. Mechtcherine, K. Khayat, E. Secrieru (Eds.) Rheology and Processing of Construction Materials, Springer International Publishing, Cham, 2020, pp. 363-372.
[162] B. Zhu, J. Pan, B. Nematollahi, Z. Zhou, Y. Zhang, J. Sanjayan, Development of 3D printable engineered cementitious composites with ultra-high tensile ductility for digital construction, Materials & Design 181 (2019) 108088.
[163] W. Zhou, Y. Zhang, L. Ma, V.C. Li, Influence of printing parameters on 3D printing engineered cementitious composites (3DP-ECC), Cement and Concrete Composites 130 (2022) 104562.
[164] N. Xu, Y. Qian, J. Yu, C.K.Y. Leung, Tensile performance of 3D-printed Strain-Hardening Cementitious Composites (SHCC) considering material parameters, nozzle size and printing pattern, Cement and Concrete Composites 132 (2022) 104601.